A-TDEP

Temperature Dependent Effective Potential for ABINIT

–

Lattice dynamic properties including anharmonicity

François Bottin[a,], Jordan Bieder[b,a], Johann Bouchet[a]*

[a] CEA, DAM, DIF, F-91297 Arpajon, France.
[b] Theoretical Materials Physics, Q-MAT, CESAM, University of Liège, B-4000 Liège, Belgium

Abstract

In this paper, we present the A-TDEP post-process code implemented in the ABINIT package. This one is able to capture the explicit thermal effects in solid state physics and to produce a large number of temperature dependent thermodynamic quantities, including the so-called anharmonic effects. Its use is straightforward and require only a single *ab initio* molecular dynamic (AIMD) trajectory. A Graphical User Interface (GUI) is also available, making the use even easier.

We detail our home made implementation of the original "Temperature Dependent Effective Potential" method proposed by Hellman *et al.* [1]. In particular, we present the various algorithms and schemes used in A-TDEP which enable to obtain the effective Interatomic Force Constants (IFC). The 2nd and 3rd order effective IFC are produced self-consistently using a least-square method, fitting the AIMD forces on a model Hamiltonian function of the displacements. In addition, we stress that we face to a constrained least-square problem since all the effective IFC have to fulfill the several symmetry rules imposed by the space group, by the translation or rotation invariances of the system and by others.

Numerous thermodynamic quantities can be computed starting from the

---

[*] Corresponding author.
E-mail address: francois.bottin@cea.fr

2nd order effective IFC. The first one is the phonon spectrum, from which a large number of other quantities flow : internal energy, entropy, free energy, specific heat... The elastic constants and other usual elastic moduli (the bulk, shear and Young moduli) can also be produced at this level. Using the 3rd order effective IFC, we show how to extract the thermodynamic Grüneisen parameter, the thermal expansion, the sound velocities... and in particular, how to take into account the anisotropy of the system within.

As representative applications of A-TDEP capabilities, we show the thermal evolution of the soft phonon mode of α-U, the thermal stabilization of the bcc phase of Zr and the thermal expansion of diamond Si. All these features highlight the strong anharmonicity included in these systems.

Keywords: Phonons; Anharmonicity; *ab initio*; Molecular Dynamics; Thermodynamics

---

PROGRAM SUMMARY/NEW VERSION PROGRAM SUMMARY

Program Title: A-TDEP
Licensing provisions(please choose one): GNU General Public License, version 3
Programming language: Fortran 2003
Supplementary material:
Nature of problem(approx. 50-250 words):
This software aims at computing thermodynamic properties at finite temperature beyond the quasi-harmonic approximation. The anharmonic effects are taken into account in an effective way in the evaluation of all the thermodynamic properties computed by this code : phonon frequencies, free energy, elastic constants, Grüneisen parameter, thermal expansion, sound velocity, thermal pressure...
Solution method(approx. 50-250 words):
The method implemented in A-TDEP is the so called Temperature Dependant Effective Potential [2, 1]. In this framework, the forces and displacements coming from an *ab initio* molecular dynamic trajectory are used to extract the second and third order effective IFC by means of a constrained least-square method.
Additional comments including Restrictions and Unusual features (approx. 50-250 words):
The software is included in the ABINIT package [3] and directly interfaced with its results through the use of a NETCDF file. Nevertheless, it is not mandatory to run the *ab initio* molecular dynamic simulations within ABINIT or to use a NETCDF input file ; the user can also provide three ASCII files (forces, positions, energies).

Introduction

The study of thermal properties of materials has always been the subject of a significant research effort in solid state physics. Whatever the purpose, experiments and theory have brought together their discoveries to understand the mechanisms that governed temperature effects. A large number of fields of research are concerned and interested in a still better description of materials when they undergo some temperature variations : astrophysics, superconductivity, aerospace industry, electronics, geoscience... All of them require the building of phase diagrams, the refinement of Equation of States (EoS) and the characterization of thermodynamic quantities.

The theory of lattice dynamics has been developed for this purpose and specifies that thermal effects can be captured by describing precisely the lattice vibrations of the system. In this framework, the key quantity is the phonon frequencies $\omega(V, T)$ which depend on the volume V and the temperature T. Within the harmonic approximation (HA), the most famous approach based on the quantum harmonic crystal, the lattice vibrations $\omega_{\mathrm{HA}}(V)$ are temperature independent and the temperature effects are only taken into account through the population of phonon states by the Bose-Einstein statistics. If this approximation has encountered many success, nevertheless this one failed to describe the thermal expansion of materials. That is the reason why another approximation has been proposed : the quasi-harmonic approximation (QHA). This one considers that the phonon frequencies depend on the temperature through the variation of the volume : $\omega_{\mathrm{QHA}}(V(T))$. Even if the temperature is not explicitly taken into account, the QHA is able to capture most of standard thermal effects encountered by materials.

However, the QHA reaches its limits when the atoms explore the anharmonic part of the potential. If this can happen at low temperature (for hydrogen and helium, for instance), this is generally encountered when materials are strongly heated, when some crystalline phases are (de)stabilized wrt temperature, when thermodynamic conditions are close to phase transitions... In these cases, an harmonic description of the potential is no longer sufficient. Moreover, if the QHA already includes some effects going beyond the harmonic approximations (the thermal expansion, for instance), it is not able to account for thermal effects at constant volume. In this case, the temperature effects not described by the harmonic approximation can be split in two parts [4, 5, 6, 7] :

- one described by the QHA, named **isothermal** or **extrinsic**, able to

describe the thermal expansion but inefficient to depict the thermal behaviour of materials at constant volume,

- another going beyond the QHA, named **isochoric** or **intrinsic**, which treats explicitly the dependency wrt the temperature and reproduces thermal effects at constant volume : $\omega_{\text{Anh}}(V(T), T)$.

One can formalize and synthesize this statement as follows :

$$\left(\frac{\partial \omega}{\partial T}\right)_p = \left(\frac{\partial \omega}{\partial T}\right)_V + \left(\frac{\partial \omega}{\partial V}\right)_T \left(\frac{\partial V}{\partial T}\right)_p \tag{1}$$

The second term of the right hand side of the previous equation is included in the QHA, but not the first one only treated when the temperature dependency is explicit.

As well for material science as for theoretical issues, the calculation of lattice vibrations (whatever the thermodynamic conditions) is becoming one of the most important challenge in solid state physics. For this purpose, the *ab initio* calculations are well suited : both the effects of pressure and temperature can be taken into account, without any assumption about the interatomic potential. Two approaches have been developed in order to compute the phonon frequencies at the harmonic level : either by brute force using finite differences [8, 9] or by employing a more elegant method, the density functional perturbation theory (DFPT) [10, 11]. If recent developments show that finite differences *ab initio* calculations are able to capture strong anharmonic effects [12, 13] it seems more challenging for DFPT to compute the terms above the cubic one [14] using the $2n + 1$ theorem [15].

Since the beginning of the 60's, several microscopic formalisms has been proposed in order to go beyond the simple quantum harmonic crystal and to deal with the anharmonic effects [16, 17, 18, 19, 20, 21, 22]. Not only do they offer a description of lattice vibrations going beyond the QHA (that is to say capturing thermal intrinsic effects) but also they give a comprehensive framework including anharmonicity in thermodynamics and elasticity. If these theoretical developments were very successful in the past sixty years, they were restricted to analytical results. Nowadays, due to the increasing power of supercomputers, they can be introduced in computational codes in order to access quantities unreachable in the past.

A large number of theoretical approaches have been developed during the last ten years in order to capture the anharmonics effects starting from

ab initio calculations. These ones have led to several computational codes which have recently emerged in the solid state physics community. Without claiming to make an exhaustive list, we can mention :

- the so-called "Self-Consistent Ab-Initio Lattice Dynamics" (SCAILD) method developed by Souvatzis *et al.* [23, 24, 25, 26],

- the famous python code for phonons calculations (PHONOPY) developed by Togo and Tanaka [9, 27, 28] and the new code (DynaPhoPy) able to extract phonon quasiparticles from AIMD simulations [29],

- the computational code named "Anharmonic LAttice MODEl" (ALAM-ODE) developed by Tadano *et al.* [30, 31, 32, 13]

- the "Stochastic Self-Consistent Harmonic Approximation" (SSCHA) developed by Errea *et al.* [33, 34, 35, 36, 37],

- the approach named "Compressive Sensing Lattice Dynamics" developed by Nelson, Zhou*et al.* [38, 39],

- the method proposed by Glensk *et al.* allowing to deduce the anharmonic contributions via a direct derivation of the Gibbs energy [40, 41, 42],

- the Automatic Anharmonic Phonon Library (AAPL) developed by Curtarolo *et al.* [43, 44]

In this work, we present an implementation of the method originally proposed by Esfarjani and Stokes [2, 45, 46] then developed by Hellman and collaborators [1, 47, 48, 49]. This one, named "Temperature Dependent Effective Potential" (TDEP), allows to extract the effective interatomic force constants (IFC) by means of AIMD simulations or through a stochastic generation of the configurations. As already highlighted by other authors, this method can be applied successfully to go beyond QHA and capture explicit thermal effects [50, 51, 52, 53, 54, 55].

If a large number of equations and definitions are already published in the literature, few details are available concerning the implementation of this method. In the following, we propose to give them in the particular case of our home-made implementation in the ABINIT code [56]. In the first section, we present the TDEP method as it is exposed in the literature. Then, we

detail its implementation in the ABINIT code and focus on the algorithms used in practice. In the following, we describe all the capabilities of the A-TDEP code ; i.e. all the thermodynamic quantities that can be computed. Finally, we show the results obtained for three prototypical materials : Si, Zr and U.

1. The Temperature Dependent Effective Potential

1.1. The Interatomic Forces Constants

Let us define a 3-dimensional crystal composed of N_a atoms i in their equilibrium positions which undergo small displacements u_i^α along the α direction. The potential energy of this system can be rewritten using a Taylor expansion around the equilibrium :

$$U = U_0 \ + \ \sum_{\substack{p \geq 1}} \frac{1}{p\,!} \sum_{\substack{\alpha_1...\alpha_p \\ i_1...i_p}} \overset{(p)}{\Phi}{}_{i_1...i_p}^{\alpha_1...\alpha_p} \prod_{k=1}^{p} u_{i_k}^{\alpha_k} \tag{2}$$

with U_0 the minimum of the potential energy. In this equation, and in the following, the Latin letters in subscripts $i, j, k, ...$ (but also $i_1,...,i_p$) and the Greek letters in superscripts $\alpha, \beta, \gamma, ...$ (but also $\alpha_1, ..., \alpha_p$) will define the atoms and the cartesian directions, respectively. In Equation 2, the first term of the development $\overset{(1)}{\Phi}{}_i^\alpha$ defines the net force acting on the atom i and is null when the expansion is performed around equilibrium positions (corresponding to the thermodynamic conditions).

At the second order, the hamiltonian includes all pair interactions between atoms i and j. This quantity $\overset{(2)}{\Phi}{}_{ij}^{\alpha\beta}$ defines the harmonic part of the potential and is called "the second order IFC" (IFC_2^{tot}).

In the same way, the third and fourth order IFC (IFC_3^{tot}, IFC_4^{tot}), also called cubic and quartic force constants, are $\overset{(3)}{\Phi}{}_{ijk}^{\alpha\beta\gamma}$ and $\overset{(4)}{\Phi}{}_{ijkl}^{\alpha\beta\gamma\delta}$. These ones contain all the three and four body interactions between the i, j, k and l atoms. When the third and fourth order terms become significant, the system acquires a truly anharmonic behavior with an asymmetric shape of the potential [57, 58, 59].

6

In this framework, the total force acting on each atom i and for each direction α is written as :

$$\mathcal{F}_{i_1}^{\alpha_1} = -\sum_{p \geq 2} \frac{1}{(p-1)!} \sum_{\substack{\alpha_2...\alpha_p \\ i_2...i_p}} \overset{(p)}{\Phi}{}_{i_1 i_2...i_p}^{\alpha_1 \alpha_2...\alpha_p} \prod_{k=2}^{p} u_{i_k}^{\alpha_k} \tag{3}$$

1.2. The principles of the TDEP method

In the TDEP method, the aim is to extract the IFC in an effective way. Now, let us assume that the previous system evolves using AIMD, and consider that N_t configurations are acquired along the trajectory. At each time step t, we can store the new positions of the atoms $\tau_{MD,i}^{\alpha}(t)$, the forces $\mathcal{F}_{MD,i}^{\alpha}(t)$ and define the displacements wrt the equilibrium positions $u_{MD,i}^{\alpha}(t) = \tau_{MD,i}^{\alpha}(t) - \overline{\tau}_{MD,i}^{\alpha}$, with $\overline{\tau}_{MD,i}^{\alpha}$ the equilibrium positions. Knowing the forces and displacements, and using Equation 3, it is possible to extract the IFC by solving the following system of equations :

$$\mathcal{F}_{MD,i_1}^{\alpha_1}(t) = -\sum_{p \geq 2}^{P} \frac{1}{(p-1)!} \sum_{\substack{\alpha_2...\alpha_p \\ i_2...i_p}} \overset{(p)}{\Theta}{}_{i_1 i_2...i_p}^{\alpha_1 \alpha_2...\alpha_p} \prod_{k=2}^{p} u_{MD,i_k}^{\alpha_k}(t) \tag{4}$$

The expansion is now performed up to the Pth order (in practice up to the 2nd, the 3rd or the 4th order). The fitting procedure employed to solve this system of equations modifies the terms below the truncation by including (in an effective way) the anharmonic contributions coming from the terms above the truncation. Therefore, the IFC are no longer constant and become temperature dependent. That is the reason why we change the notation : in the following, the $\overset{(p)}{\Phi}{}_{i...l}^{\alpha...\delta}$ will be referred to as the "true IFC" and the $\overset{(p)}{\Theta}{}_{i...l}^{\alpha...\delta}$ as the "effective IFC".

By rewriting Eq. 4 as a function of all IFC coefficients (we will show in the following section how to achieve it) we otain :

$$\mathcal{F}_{MD,i}^{\alpha}(t) = \sum_{p \geq 2}^{P} \sum_{\lambda} f_{i,p\lambda}^{\alpha}(\mathbf{u}_{MD}(t))\theta_{p\lambda} \tag{5}$$

with $\theta_{p\lambda}$ the λth coefficient of the IFC$_p^{tot}$ matrix and $f_{i,p\lambda}^{\alpha}(\mathbf{u}_{MD}(t))$ the function including all the displacements (but also the factorial and the minus sign).

The system of equations is now linear and has the form $A.x = b$, with A the function including all the displacements, b the forces and x the IFC

coefficients to determine. When the MD trajectory is sufficiently long, this system is overdetermined; i.e. there are more equations than unknowns. One can solve this system of equations by searching its least squares solution. Let us define the residual :

$$\mathcal{R} = \mathbf{F}_{MD} - \mathbf{f}.\Theta \tag{6}$$

such as $\mathbf{F}_{MD} \equiv \mathcal{F}_{MD,i}^{\alpha}(t)$, $\mathbf{f} \equiv f_{i,p\lambda}^{\alpha}(\mathbf{u}_{MD}(t))$ and $\Theta \equiv \theta_{p\lambda}$. One measure of smallness of $\mathcal{R}$ is to choose $\theta_{p\lambda}$ such that the sum of squares of residual $\mathcal{S}$ is as small as possible :

$$\mathcal{S} = \min(\mathcal{R}^T.\mathcal{R}) = ||\mathbf{F}_{MD} - \mathbf{f}.\Theta||^2 \tag{7}$$

The solution giving the lowest residual (i.e. the IFC coefficients giving the best fit of the MD forces) is the following least squares solution :

$$\Theta = \mathbf{f}^{\dagger}.\mathbf{F}_{MD} \tag{8}$$

with $\mathbf{f}^{\dagger}$ the pseudoinverse of the $\mathbf{f}$ matrix. This latter is a generalization of the inverse matrix and we will see at the end of the next section how to compute it.

1.3. How many coefficients in the effective IFC?

If the system is composed of N_a atoms, the effective IFC contain $(3N_a)^p$ coefficients at the pth order, so one has to compute $\sum_{p=1}^{4}(3N_a)^p$ coefficients at the fourth order. On the other hand, at each time step of the MD simulation one accumulates $3N_a$ equations. Therefore, if one wants to acquire "at least" as many equations as unknowns, the MD trajectory have to contain $N_t = \sum_{p=1}^{4}(3N_a)^{p-1}$ time steps. For instance, if one considers a supercell with 100 atoms, it is needed to have "at least" N_t=90 301 time steps in order to compute the 27 090 300 coefficients up to the third order.

These few lines unveil the problematic. The calculation of the whole IFC_p^{tot} matrices is possible but at a prohibitive computational cost. Moreover, the goal is to have an overdetermined system of linear equations in order to solve it by means of a least-squares method.

Here, we show an expansion of the second order effective IFC, solution of

8

the system of equations :

$$
\begin{pmatrix}
\mathcal{F}_1^x(t) \\
\mathcal{F}_1^y(t) \\
\mathcal{F}_1^z(t) \\
\mathcal{F}_2^x(t) \\
\mathcal{F}_2^y(t) \\
\mathcal{F}_2^z(t) \\
\vdots \\
\mathcal{F}_{N_a}^z(t)
\end{pmatrix}
= -
\begin{pmatrix}
\begin{pmatrix} \theta_{21} & 0 & 0 \\ 0 & \theta_{21} & 0 \\ 0 & 0 & \theta_{21} \end{pmatrix} & \begin{pmatrix} \theta_{22} & \theta_{23} & \theta_{24} \\ -\theta_{23} & \theta_{22} & \theta_{26} \\ \theta_{25} & \theta_{26} & \theta_{22} \end{pmatrix} & \cdots \\
\begin{pmatrix} \theta_{22} & -\theta_{23} & \theta_{25} \\ \theta_{23} & \theta_{22} & \theta_{26} \\ \theta_{24} & \theta_{26} & \theta_{22} \end{pmatrix} & \begin{pmatrix} \theta_{27} & 0 & 0 \\ 0 & \theta_{27} & 0 \\ 0 & 0 & \theta_{27} \end{pmatrix} & \cdots \\
\cdots \quad \cdots \quad \cdots & \cdots \quad \cdots \quad \cdots & \ddots
\end{pmatrix}
\begin{pmatrix}
u_1^x(t) \\
u_1^y(t) \\
u_1^z(t) \\
u_2^x(t) \\
u_2^y(t) \\
u_2^z(t) \\
\vdots \\
u_{N_a}^z(t)
\end{pmatrix}
$$

The whole $3N_a \times 3N_a$ matrix is symmetric. Each 3×3 pair interaction (see for example the $\begin{pmatrix} \theta_{22} & \theta_{23} & \theta_{24} \\ -\theta_{23} & \theta_{22} & \theta_{26} \\ \theta_{25} & \theta_{26} & \theta_{22} \end{pmatrix}$ matrix) can exhibit some symmetric, antisymmetric, non-symmetric or null terms. Actually, the thousands of coefficients of the IFC_p^{tot} can be strongly reduced. If a significant effort is made upstream of the resolution process by taking into account all the symmetries, the method shown previously then becomes tractable. The five symmetry rules, responsible for the decrease of several orders of magnitude, are detailed in the following.

2. How to reduce the number of IFC coefficients?

2.1. The IFC tensors are symmetric

The energy conservation law impose that the IFC_p^{tot} tensors comply with the usual transposition rule :

$$
\overset{(2)}{\Theta}_{ij}^{\alpha\beta} = \overset{(2)}{\Theta}_{ji}^{\beta\alpha}
$$

$$
\overset{(3)}{\Theta}_{ijk}^{\alpha\beta\gamma} = \overset{(3)}{\Theta}_{jki}^{\beta\gamma\alpha} = \overset{(3)}{\Theta}_{kij}^{\gamma\alpha\beta} = \overset{(3)}{\Theta}_{ikj}^{\alpha\gamma\beta} = \overset{(3)}{\Theta}_{jik}^{\beta\alpha\gamma} = \overset{(3)}{\Theta}_{kji}^{\gamma\beta\alpha}
$$

$$
\overset{(4)}{\Theta}_{ijkl}^{\alpha\beta\gamma\delta} = \overset{(4)}{\Theta}_{jkli}^{\beta\gamma\delta\alpha} = \overset{(4)}{\Theta}_{klij}^{\gamma\delta\alpha\beta} = \overset{(4)}{\Theta}_{iklj}^{\alpha\gamma\delta\beta} = \overset{(4)}{\Theta}_{jikl}^{\beta\alpha\gamma\delta} = \overset{(4)}{\Theta}_{klji}^{\gamma\delta\beta\alpha} = \dots
$$

This invariance under the permutation of the indices is easy to implement. The total number of coefficients is divided by 2 for the IFC_2^{tot}, 6 for the IFC_3^{tot} and 24 for the IFC_4^{tot}.

2.2. The acoustic sum rule

The momentum conservation principle implies that there is no mass center displacement. To write this condition properly we split up the atomic index and expand the atomic coordinates as follows : $\boldsymbol{\tau}_i(a) = \mathbf{r}_i + \mathbf{R}(a)$ with $\mathbf{r}_i$ the atomic position of the atom i in the cell 0 and $\mathbf{R}(a)$ the lattice vector of the cell a. In this framework, the acoustic sum rule writes [2, 45] :

$$\sum_i \overset{(1)}{\Theta}{}_i^\alpha(0) = 0 \quad \forall\,(\alpha)$$

$$\sum_{jb} \overset{(2)}{\Theta}{}_{ij}^{\alpha\beta}(0,b) = 0 \quad \forall\,(i,\alpha\beta)$$

$$\sum_{kc} \overset{(3)}{\Theta}{}_{ijk}^{\alpha\beta\gamma}(0,b,c) = 0 \quad \forall\,(ijb,\alpha\beta\gamma)$$

$$\sum_{ld} \overset{(4)}{\Theta}{}_{ijkl}^{\alpha\beta\gamma\delta}(0,b,c,d) = 0 \quad \forall\,(ijkbc,\alpha\beta\gamma\delta)$$

with $\overset{(p)}{\Theta}{}_{i_1...i_p}^{\alpha_1...\alpha_p}(a_1,...,a_p)$ the effective IFC at the pth order corresponding to the interaction between the $(i_1^{th},...,i_p^{th})$ atoms in cells $(a_1,...,a_p)$, respectively. These equations lead to some relations between all the coefficients of each IFC. By using some mathematics (and contracting the summation index over atoms), it can be showed that Equation 3 can be rewritten as :

$$\mathcal{F}_i^\alpha = -\overset{(1)}{\Theta}{}_i^\alpha \; - \; \sum_{\beta,j\neq i} \overset{(2)}{\Theta}{}_{ij}^{\alpha\beta}(u_j^\beta - u_i^\beta)$$

$$- \; \frac{1}{2} \sum_{\substack{\beta\gamma \\ j\neq i,k\neq i}} \overset{(3)}{\Theta}{}_{ijk}^{\alpha\beta\gamma}(u_j^\beta - u_i^\beta)(u_k^\gamma - u_i^\gamma)$$

$$- \; \frac{1}{6} \sum_{\substack{\beta\gamma\delta \\ j\neq i,k\neq i,l\neq i}} \overset{(4)}{\Theta}{}_{ijkl}^{\alpha\beta\gamma\delta}(u_j^\beta - u_i^\beta)(u_k^\gamma - u_i^\gamma)(u_j^\delta - u_i^\delta)$$

$$(9)$$

We can easily see that, at each order, the on-site coefficients are not involved in the calculation of the total force and that the invariance of the system

under arbitrary translation is fully achieved. The constraints coming from the acoustic sum rules lead to a reduction of the IFC coefficients and we will show in Section 2.7 how to proceed.

2.3. The rotational invariance

The system (force and energy) has to remain invariant after a rotation. This imposes some relations between the IFC of different orders [2, 45] :

$$
0 = \sum_{i,\alpha\beta} \overset{(1)}{\Theta}{}_i^\alpha(0)\tau_i^\beta \epsilon^{\alpha\beta\nu} \quad \forall\, (\nu)
$$

$$
0 = \sum_{jb,\beta\gamma} \overset{(2)}{\Theta}{}_{ij}^{\alpha\beta}(0,b)\tau_j^\gamma \epsilon^{\beta\gamma\nu} + \sum_\beta \overset{(1)}{\Theta}{}_i^\beta(0)\epsilon^{\beta\alpha\nu} \quad \forall\, (i,\alpha\nu)
$$

$$
0 = \sum_\gamma \overset{(2)}{\Theta}{}_{ij}^{\gamma\beta}(0,b)\epsilon^{\gamma\alpha\nu} + \sum_\gamma \overset{(2)}{\Theta}{}_{ij}^{\alpha\gamma}(0,b)\epsilon^{\gamma\beta\nu}
$$

$$
+ \sum_{kc,\gamma\delta} \overset{(3)}{\Theta}{}_{ijk}^{\alpha\beta\gamma}(0,b,c)\tau_k^\delta \epsilon^{\gamma\delta\nu} \quad \forall\, (ijb,\alpha\beta\nu)
$$

$$
0 = \sum_\delta \overset{(3)}{\Theta}{}_{ijk}^{\delta\beta\gamma}(0,b,c)\epsilon^{\delta\alpha\nu} + \sum_\delta \overset{(3)}{\Theta}{}_{ijk}^{\alpha\delta\gamma}(0,b,c)\epsilon^{\delta\beta\nu} + \sum_\delta \overset{(3)}{\Theta}{}_{ijk}^{\alpha\beta\delta}(0,b,c)\epsilon^{\delta\gamma\nu}
$$

$$
+ \sum_{ld,\delta\mu} \overset{(4)}{\Theta}{}_{ijkl}^{\alpha\beta\gamma\delta}(0,b,c,d)\tau_l^\mu \epsilon^{\delta\mu\nu} \quad \forall\, (ijkbc,\alpha\beta\gamma\nu)
$$

with $\epsilon^{\alpha\beta\gamma}$ the Levi-Civita symbols. As for the acoustic sum rules defined in the previous subsection, one explains in Section 2.7 how to impose such constraints.

2.4. The crystal symmetries (I)

Using the crystal symmetry operations $\mathcal{S}$, it is possible to pursue the reduction process of the IFC coefficients:

- by deducing all the IFC$_p$ connected to a reference IFC$_p^{ref}$ through a crystal symmetry (that is the subject of this section). In this case, the symmetries $\mathcal{S}$ used are the space group operations (mirrors, rotations, translations including non-symmorphic ones).

11
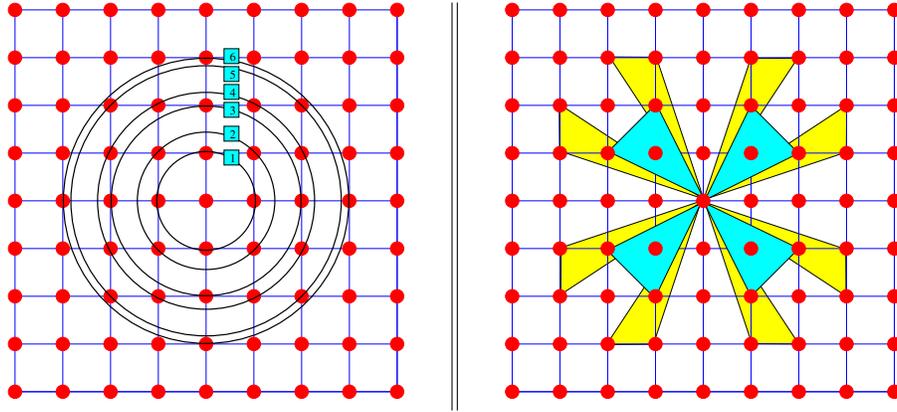
Figure 1: Sketch of interaction shells in 2-dimension. Left panel (second order) : six shells of pair interaction. The atoms belonging to each shell are connected through the crystal symmetries. Right panel (third order) : two kinds of triplet interactions.

- by determining the nonzero coefficients really independent in the IFC_p^{ref} (this will be the subject of the next section). In this case, the symmetries $\mathcal{S}$ used are the point group operations.

By means of space group operations, it is possible to deduce all the interactions from a set of reference ones. Schematically, this reduction is achieved using simultaneously two kinds of operations : by taking into account the translations, it reduces the complexity of the supercell to the first unitcell at most, and by considering the mirrors and rotations, it is possible to build some shells of interaction (see Figure 1) around reference atoms in the first unitcell. Therefore, using the symmetry operation $\mathcal{S}$, each "image" interaction, with the atoms indexed by the $\mathcal{S}(i)...\mathcal{S}(l)$ letters, can be deduced from

a "reference" interaction involving the atoms $i...l$, such as :

$$\overset{(1)}{\Theta}{}^{\alpha}_{\mathcal{S}(i)} = \sum_{\mu} \mathcal{S}^{\alpha\mu} \overset{(1)}{\Theta}{}^{\mu}_{i} \tag{10}$$

$$\overset{(2)}{\Theta}{}^{\alpha\beta}_{\mathcal{S}(i)\mathcal{S}(j)} = \sum_{\mu\nu} \mathcal{S}^{\alpha\mu} \mathcal{S}^{\beta\nu} \overset{(2)}{\Theta}{}^{\mu\nu}_{ij} \tag{11}$$

$$\overset{(3)}{\Theta}{}^{\alpha\beta\gamma}_{\mathcal{S}(i)\mathcal{S}(j)\mathcal{S}(k)} = \sum_{\mu\nu\xi} \mathcal{S}^{\alpha\mu} \mathcal{S}^{\beta\nu} \mathcal{S}^{\gamma\xi} \overset{(3)}{\Theta}{}^{\mu\nu\xi}_{ijk} \tag{12}$$

$$\overset{(4)}{\Theta}{}^{\alpha\beta\gamma\delta}_{\mathcal{S}(i)\mathcal{S}(j)\mathcal{S}(k)\mathcal{S}(l)} = \sum_{\mu\nu\xi o} \mathcal{S}^{\alpha\mu} \mathcal{S}^{\beta\nu} \mathcal{S}^{\gamma\xi} \mathcal{S}^{\delta o} \overset{(4)}{\Theta}{}^{\mu\nu\xi o}_{ijkl} \tag{13}$$

The number of coefficients falls down significantly after this work. If 10 shells of pair interactions are present, there are at worst $3^2 * 10 = 90$ coefficients to determine for the second order... and no longer $(3*N_a)^2 = 90\ 000$ as before.

2.5. The crystal symmetries (II)

The last symmetry rule is probably the most subtle and tedious to carry out. The aim of this subsection is to obtain *a priori* the exact number of nonzero coefficients really independent in the reference matrices IFC^{ref}_p. The symmetry operations $\mathcal{S}$ used here belong to the point group, which forms a subgroup of the orthogonal group. Consequently, all the symmetry operations $\mathcal{S}$ (in the cartesian space) belonging to this group have the following properties :

- The inverse equals its transpose : $\mathcal{S}^{-1} = \mathcal{S}^{\mathrm{T}}$

- The norm of the (three) eigenvalues equals to 1: $\lambda = (\pm 1, \pm 1, \pm 1)$ when $\mathcal{S}$ is symmetric, or $\lambda = (\pm 1, e^{i\theta}, e^{-i\theta})$ when $\mathcal{S}$ is antisymmetric.

- The norm of the (three) eigenvectors equals to 1: $|p| = 1$

These properties will be used thereafter and will strongly simplify the development. We have to consider two peculiar cases : some symmetry operations $\mathcal{S}$ may let the interaction invariant and/or some others may reverse the interaction. This imposes some constraints on the IFC and thus reduces the number of coefficients. Note that the symmetry operations leaving the interaction invariant (or reversed) form a subgroup of the point group, so a

13

large set of constraints may consistently act on the IFC. In the following, we restrict the development to the second order. The reasoning is the same for all the others.

If the symmetry leaves the bond invariant.... the IFC_2^{ref} is not affected by the transformation, so $\mathcal{S}(i) = i$ and $\mathcal{S}(j) = j$ in Equation 11 which becomes :

$$\overset{(2)}{\Theta}{}_{ij}^{\alpha\beta} = \sum_{\mu\nu} \mathcal{S}^{\alpha\mu}\mathcal{S}^{\beta\nu}\overset{(2)}{\Theta}{}_{ij}^{\mu\nu}$$

We can apply the eigenvectors of the $\mathcal{S}$ symmetry operation and obtain :

$$\sum_{\alpha\beta} p_r^\alpha p_s^\beta \overset{(2)}{\Theta}{}_{ij}^{\alpha\beta} = \lambda_r^\star \lambda_s^\star \sum_{\mu\nu} p_r^\mu p_s^\nu \overset{(2)}{\Theta}{}_{ij}^{\mu\nu} \quad \forall (r, s = 1, 2, 3)$$

By gathering the left and right members we get:

$$(\lambda_r^\star \lambda_s^\star - 1) \sum_{\alpha\beta} p_r^\alpha p_s^\beta \overset{(2)}{\Theta}{}_{ij}^{\alpha\beta} = 0 \quad \forall (r, s = 1, 2, 3)$$

The left hand-side of the equation equals to zero if $i)$ the term between brackets is null or if $ii)$ the summation is null. The eigenvalues of $\mathcal{S}$ being equal to ± 1 or $e^{\pm i\theta}$, it happens very frequently that their product equals to 1. Consequently, the condition $i)$ and the previous equality is naturally fulfilled in numerous cases. Otherwise, we have :

$$\sum_{\alpha\beta} p_r^\alpha p_s^\beta \overset{(2)}{\Theta}{}_{ij}^{\alpha\beta} = 0 \quad \text{if} \quad \lambda_r^\star \lambda_s^\star \neq 1 \quad \forall (r, s = 1, 2, 3) \tag{14}$$

These equations impose some constraints on the IFC_2^{ref} (linear relation between the coefficients). We will see in the following how to extract the nonzero independent coefficients.

If the symmetry reverses the bond.... the permutation also affects IFC_2^{ref}, so $\mathcal{S}(i) = j$ and $\mathcal{S}(j) = i$ in Equation 11 which becomes :

$$\overset{(2)}{\Theta}{}_{ji}^{\alpha\beta} = \sum_{\mu\nu} \mathcal{S}^{\alpha\mu}\mathcal{S}^{\beta\nu}\overset{(2)}{\Theta}{}_{ij}^{\mu\nu}$$

Using the symmetry properties of the IFC then by applying the eigenvectors and gathering the left and right hand-side, one obtains :

$$\sum_{\alpha\beta}(\lambda_r^\star\lambda_s^\star p_r^\alpha p_s^\beta - p_r^\beta p_s^\alpha)\overset{(2)}{\Theta}{}_{ij}^{\alpha\beta} = 0 \quad \forall(r,s=1,2,3) \tag{15}$$

As already highlighted when the interaction is kept invariant, these equations also impose some constraints if the term within brackets is not null.

2.6. All the symmetries together

For each order and shell independently, all the equations (see equations 14 and 15) are collected then orthonormalized, resulting in a system of Λ_p independent homogeneous linear equations (at the pth order). This system may be rewritten as :

$$\sum_{\kappa=1}^{3^p}\Upsilon_{\lambda_p}^\kappa\overset{(p)}{\Theta}{}_{i_1...i_p}^\kappa = 0 \quad \text{with } \lambda_p = 1,...\Lambda_p$$

with the superscripts $\alpha_1...\alpha_p$ contracted in κ, and the matrix $\Upsilon_{\lambda_p}^\kappa$ coming from all the nonzero terms between brackets. The solutions of such system is obtained by computing the kernel of the application. The result has the following form :

$$\overset{(p)}{\Theta}{}_{i_1...i_p}^\kappa = \sum_{\lambda_p=1}^{\Lambda_p}\Upsilon_{\lambda_p}'^\kappa\theta_{p\lambda_p} \quad \text{with } \kappa=1,...3^p$$

with $\theta_{p\lambda_p}$ the Λ_p nonzero independent coefficients of the IFC$_p^{ref}$. The $\Upsilon_{\lambda_p}'^\kappa$ matrix is built by gathering the column vectors orthogonal to the line vectors of $\Upsilon_{\lambda_p}^\kappa$.

By taking into account all the interactions of each shell at each order, we finally recover Equation 5 : $\mathcal{F}_i^\alpha(t) = \sum_{p\lambda_p} f_{i,p\lambda_p}^\alpha(\mathbf{u}(t))\theta_{p\lambda_p}$. All the terms depending on the displacements $u_i^\alpha(t)$ and symmetries $S^{\alpha\beta}$ are hidden in the $\mathbf{f}$ matrix. We obtain a system of linear equations with the nonzero coefficients

of the effective IFC $\{\theta^{p\lambda_p}\}$ as the unknown variables. Its expanded form is :

$$
\begin{pmatrix}
\mathcal{F}_1^x(1) \\
\mathcal{F}_1^y(1) \\
\mathcal{F}_1^z(1) \\
\vdots \\
\mathcal{F}_{N_a}^z(1) \\
\vdots \\
\mathcal{F}_{N_a}^z(N_t)
\end{pmatrix}
=
\begin{pmatrix}
f_{1,11}^x(1) & f_{1,12}^x(1) & \cdots & f_{1,p\Lambda_p}^x(1) \\
f_{1,11}^y(1) & f_{1,12}^y(1) & \cdots & f_{1,p\Lambda_p}^y(1) \\
f_{1,11}^z(1) & f_{1,12}^z(1) & \cdots & f_{1,p\Lambda_p}^z(1) \\
\vdots & \vdots & \vdots & \vdots \\
f_{N_a,11}^z(1) & f_{N_a,12}^z(1) & \cdots & f_{N_a,p\Lambda_p}^z(1) \\
\vdots & \vdots & \vdots & \vdots \\
f_{N_a,11}^z(N_t) & f_{N_a,12}^z(N_t) & \cdots & f_{N_a,p\Lambda_p}^z(N_t)
\end{pmatrix}
\begin{pmatrix}
\theta_{11} \\
\theta_{12} \\
\theta_{13} \\
\vdots \\
\theta_{1\Lambda_1} \\
\vdots \\
\theta_{p\Lambda_p}
\end{pmatrix}
$$

We stress that the **f** matrix is really huge. At the second order, its size is $(3 * N_a * N_t) \times \Lambda_2$. If we consider N_t=1000 time steps, N_a=100 atoms and Λ_2=20 coefficients, this matrix has 300 000 lines and 20 columns.

2.7. The constrained least squares problem

The whole set of coefficients $\{\theta_{p\lambda_p}\}$ can be obtained by reversing the previous equation. An elegant way [2, 1] to perform such reversion is to compute the Moore-Penrose pseudoinverse (marked with a † superscript in the following, see Equation 8):

$$
\begin{pmatrix}
\theta_{11} \\
\vdots \\
\theta_{p\Lambda_p}
\end{pmatrix}
=
\begin{pmatrix}
f_{1,11}^x(1) & \cdots & f_{1,p\Lambda_p}^x(1) \\
\vdots & \ddots & \vdots \\
f_{N_a,11}^z(N_t) & \cdots & f_{N_a,p\Lambda_p}^z(N_t)
\end{pmatrix}^\dagger
\cdot
\begin{pmatrix}
\mathcal{F}_1^x(1) \\
\vdots \\
\mathcal{F}_{N_a}^z(N_t)
\end{pmatrix}
$$

The usual and mathematical definition of a pseudoinverse $\Gamma^\dagger$ is :

$$
\Gamma^\dagger = \Gamma^T (\Gamma.\Gamma^T)^{-1} \tag{16}
$$

This definition implies to carry out a reversion of the **f** matrix. In practice, this method is proved to be numerically unstable and the computational cost turn out to be really expensive, due to the size of the matrix. A more simple and accurate way is possible, by performing a singular value decomposition :

$$
\Gamma^\dagger = \mathcal{V}.\Sigma^\dagger.\mathcal{U}^T \tag{17}
$$

with $\mathcal{V}$ and $\mathcal{U}$ some square matrices and Σ a diagonal matrix. Some linear algebra routines (`dgesdd`) enable to perform such decomposition easily. The

Σ being diagonal, this one can be conveniently reversed, which makes this method much more stable and less expensive than the previous one.

We have seen previously that the acoustic sum rules and the rotational invariance of the system impose some constraints on the IFC. In the same way, we will see in the following that the dynamical matrix and the elastic tensor also impose other constraints on IFC. If one rewrites these Q linear constraints, function of the $\theta_i \equiv \theta_{p\lambda_p}$ coefficients, in a matrix $\mathbf{C}$, we obtain an homogeneous linear equation system :

$$\sum_{i=1}^{p\Lambda_p} C_{q,i}^T \theta_i = 0 \quad \text{with } q = 1, ..., Q \tag{18}$$

In order to satisfy these constraints we have to :

1. minimize $\mathcal{S} = ||\mathbf{F}_{MD} - \mathbf{f}.\mathbf{\Theta}||^2$, as previously performed by least squares method with Eq.7

2. subject to $\mathbf{C}.\mathbf{\Theta} = 0$.

That can be done by building the Lagrangian function $\mathcal{L}(\theta, \zeta)$ with ζ the Lagrange multipliers :

$$\mathcal{L}(\theta, \zeta) = \mathcal{S}(\theta) + \sum_{q=1}^{Q} \zeta_q \sum_{i=1}^{p\Lambda_p} C_{q,i}^T \theta_i \tag{19}$$

The optimality conditions are :

$$\begin{cases} \frac{\partial \mathcal{L}}{\partial \theta_i} = & 2\sum_{j=1}^{p\Lambda_p}(\mathbf{f}^T.\mathbf{f})_{ij}\theta_j - 2(\mathbf{f}^T.\mathbf{F}_{MD})_i + \sum_{q=1}^{Q} \zeta_q C_{q,i} = 0 \\ \frac{\partial \mathcal{L}}{\partial \zeta_q} = & \sum_{q=1}^{Q} C_{q,i}^T \theta_i = 0 \end{cases}$$

In matrix-vector form, these equations are more readable and are written :

$$\begin{pmatrix} 2\mathbf{f}^T.\mathbf{f} & \mathbf{C}^T \\ \mathbf{C} & 0 \end{pmatrix} \cdot \begin{pmatrix} \mathbf{\Theta} \\ \zeta \end{pmatrix} = \begin{pmatrix} 2\mathbf{f}^T.\mathbf{F}_{MD} \\ 0 \end{pmatrix} \tag{20}$$

As already carried out for the least square problem, the constrained least squares (CLS) solution can be obtained by computing the pseudoinverse of the first matrix in the left hand-side member. Note that the matrix to invert

is smaller than the one shown previously. At the second order, its size is $(\Lambda_2 + Q) \times (\Lambda_2 + Q)$. This one no longer depends on the number of time steps and atoms. For $\Lambda_2=20$ coefficients and $Q=5$ constraints this matrix has only 25 lines and columns.

In conclusion, we have shown in this section how to strongly reduce the number of IFC coefficients using symmetries and invariances of the system. In this implementation, the CLS method used to compute the IFC coefficients is applied only once (for all orders simultaneously) and all the IFC coefficients are obtained together. Consequently, the 2nd order effective IFC may change depending on whether the 3rd and/or 4th order is included or not in the CLS resolution. This strategy could be problematic if the Taylor expansion is divergent (when the 3rd and/or 4th order become larger than the 2nd order). One way to overcome this break down is to solve each order, one after eachother. The procedure is to compute the residual of the forces at the nth order, then apply the CLS method and evaluate the $(n+1)^{th}$ effective IFC. In this case the 2nd order effective IFC no longer changes depending on whether highest order are included or not in the expansion. In a future version of this code, we will introduce this new strategy and let the user choose to solve all the orders simultaneously or successively.

3. What are the effective IFC useful for?

In this section we show that the knowledge of effective IFC allows us to calculate a large number of physical quantities that characterize a material: phonon spectrum, free energy, elastic constants and moduli, sound speed, Grüneisen parameter, thermal expansion... Since the effective IFC are temperature dependent, all the quantities resulting from them exhibit an explicit dependence with respect to temperature.

3.1. The phonon spectrum

In order to evaluate the phonon spectrum and the vibrational density of states, we need to split up again the index over atoms as perform in the subsection 2.2. Once the $\overset{(2)}{\Theta}{}^{\alpha\beta}_{ij}(a,b)$ tensor is built (after the Moore-Penrose), it is quite direct to compute the phonons modes of the system by performing

18

its Fourier Transform. We obtain the so-called dynamical matrix :

$$D_{ij}^{\alpha\beta}(\mathbf{q}) = \sum_b \frac{\overset{(2)}{\Theta}_{ij}^{\alpha\beta}(0,b)}{\sqrt{M_i M_j}} \exp\left(i\mathbf{q}.[\mathbf{R}(b) - \mathbf{R}(0)]\right) \tag{21}$$

with $\mathbf{q}$ a wave vector belonging to the Brillouin zone (BZ) and M_i the mass of atom i. Such equations of motion can be diagonalized in order to obtain the phonon eigen frequencies $\omega_s(\mathbf{q})$ and eigen modes $X_{is}^{\alpha}(\mathbf{q})$ of the lattice :

$$\sum_{\beta,j} D_{ij}^{\alpha\beta}(\mathbf{q}) X_{js}^{\beta}(\mathbf{q}) = \omega_s^2(\mathbf{q}) X_{is}^{\alpha}(\mathbf{q}) \tag{22}$$

In this equation (representative of an harmonic oscillator) the quantum number s refers to the quantification of the eigen frequencies, with $3 * N_a$ energy levels at all. Note that the phonon spectrum depends on the presence/absence of the higher terms in the model.

The vibrational Density Of States (vDOS) $g(\omega)$ is defined by :

$$g(\omega) = \frac{1}{3N_a} \sum_{s=1}^{3N_a} \sum_{\mathbf{q}\in BZ} \delta(\omega - \omega_s(\mathbf{q})) \quad \text{such as} \quad \int_0^{\omega_{max}} g(\omega)d\omega = 1 \tag{23}$$

with ω_{max} the highest phonon frequency of the system.

3.2. Thermodynamic quantities

When one wants to evaluate the free energy $F(V,T)$ of a system as a function of the temperature and the volume, the ususal process is to split up the cold and vibrational contributions such as :

$$F(V,T) = U_0(V) + F_{\text{vib}}(V,T) \tag{24}$$

with $U_0(V)$ the zero temperature energy of the system and $F_{\text{vib}}(V,T)$ the vibrational free energy. If the cold contribution can be estimated through an independent ground state calculation, this one can also be computed as the average over time steps of the difference between the the total energy $U_{\text{MD}}(t)$ coming from the AIMD simulation and the expansion of the energy as defined by Equation 2 :

$$U_0(V) = \left\langle U_{\text{MD}}(t) - \sum_{p=1}^P \frac{1}{p!} \sum_{\substack{\alpha_1...\alpha_p \\ i_1...i_p}} \overset{(p)}{\Theta}_{i_1...i_p}^{\alpha_1...\alpha_p} \prod_{k=1}^p u_{MD,i_k}^{\alpha_k}(t) \right\rangle \tag{25}$$

19

with $\langle\rangle = \frac{1}{N_t}\sum_{t=1}^{N_t}$. If there is no strong modification of the equilibrium structure of the crystal due to temperature effects, these two approaches have to give similar results.

Concerning the vibrational part of the free energy F_{vib} (see Equation 24) but also in a similar way for the internal energy U_{vib}, the constant-volume specific heat $C_{\text{vib,V}} = \left(\frac{\partial U}{\partial T}\right)_V$ and the entropy $S_{\text{vib}} = -\left(\frac{\partial F_{\text{vib}}}{\partial T}\right)_V$, they can be evaluated in the framework of the three-dimensional quantum harmonic crystal using the vDOS [60] :

$$F_{\text{vib}} = \frac{3N_a}{\beta}\int_0^{\omega_{max}} \ln\left(2\sinh(\frac{\beta\hbar\omega}{2})\right)g(\omega)d\omega \tag{26}$$

$$U_{\text{vib}} = 3N_a\int_0^{\omega_{max}} \frac{\hbar\omega}{2}\coth(\frac{\beta\hbar\omega}{2})g(\omega)d\omega \tag{27}$$

$$C_{\text{vib,V}} = 3N_a k_B\int_0^{\omega_{max}} \left(\frac{\beta\hbar\omega}{2\sinh(\frac{\beta\hbar\omega}{2})}\right)^2 g(\omega)d\omega \tag{28}$$

$$S_{\text{vib}} = 3N_a k_B\int_0^{\omega_{max}} \left[\frac{\beta\hbar\omega}{2}\coth(\frac{\beta\hbar\omega}{2}) - \ln\left(2\sinh(\frac{\beta\hbar\omega}{2})\right)\right]g(\omega)d\omega \tag{29}$$

with $\beta = k_B T$. Note that these formulas (and the others thereafter in this section) are the common harmonic expressions and have to be modified in order to include the corrections coming from the third and fourth orders [16, 61, 62, 18, 63, 64, 65]. This work is in progress and will be achieved for a next release of the code. In a similar way [66], one can also compute the mean square displacement :

$$< u^2 > = \frac{3\hbar}{2M_a}\int_0^{\omega_{max}} \coth(\frac{\beta\hbar\omega}{2})\frac{g(\omega)}{\omega}d\omega \tag{30}$$

All these thermodynamic quantities display three kinds of dependence with respect to the temperature. The first one is given by β and originates from the Bose-Einstein statistic and corresponds to the filling of the energy levels (including the zero-point energy), another one ($\omega(V(T))$) more implicit is provided by the thermal expansion of the volume, and a last one ($\omega(T)$) is due to the explicit dependence of the phonon frequencies with respect to the temperature. If the first one is taken into account in a quantum harmonic approach, the second one appears when considering the QHA approximation, and the third one comes from the explicit treatment of the temperature carried out in this work.

3.3. Elastic constants and moduli

The effective IFC enable to obtain almost all the thermal elastic properties of a material. The elastic constants are defined using the Hooke law which relies on the strain tensor $\epsilon_{\alpha\beta}$ to the stress one $\sigma_{\gamma\delta}$, through the elastic tensor $C_{\alpha\beta\gamma\delta}$:

$$\sigma_{\alpha\beta} = C_{\alpha\beta\gamma\delta}\,\epsilon_{\gamma\delta} \tag{31}$$

The most famous way employed to compute the elastic tensor is the finite differences method. This approach, coupled with AIMD simulations, enable to take into account temperature effects. But numerous simulations have to be performed and the computational time can be prohibitive (in order to have long AIMD trajectories). Another approach is to compute phonons as a function of temperature and to evaluate the elastic constants using the slopes of the acoustic branches. This one is connected to a more elegant formulation using the IFC [16, 22]. Following D.C. Wallace [22], let us define the $A_{\alpha\beta\gamma\delta}$ quantity :

$$A_{\alpha\beta\gamma\delta} = \frac{1}{2V} \sum_{ij} \overset{(2)}{\Theta}{}_{ij}^{\alpha\beta} d_{ij}^{\gamma} d_{ij}^{\delta} \quad \text{with } d_{ij}^{\gamma} = \tau_i^{\gamma} - \tau_j^{\gamma} \tag{32}$$

The elastic constants are then obtained by using this simple following equation :

$$C_{\alpha\beta\gamma\delta} = A_{\alpha\gamma\beta\delta} + A_{\beta\gamma\alpha\delta} - A_{\alpha\beta\gamma\delta} \tag{33}$$

Using the Voigt notation and the Voigt formulation, we can define the isothermal Bulk K_T and Shear G moduli (but also the Young modulus E and the Poisson's ratio ν) as follows :

$$K_T = ((C_{11} + C_{22} + C_{33}) + 2(C_{12} + C_{13} + C_{23}))/9 \tag{34}$$
$$G = ((C_{11} + C_{22} + C_{33}) - (C_{12} + C_{13} + C_{23}) + 3(C_{44} + C_{55} + C_{66}))/15 \tag{35}$$

It is important to note that this method needs to have long range IFC in order to have converged quantities [67].

3.4. Grüneisen parameter & thermal expansion

As well known, the thermal expansion $\alpha_V = \frac{1}{V}\left(\frac{\partial V}{\partial T}\right)_P$, the thermodynamic Grüneisen parameter $\gamma = V\left(\frac{\partial P}{\partial U}\right)_V$, the isothermal compressibility

$\beta_T = -\frac{1}{V}\left(\frac{\partial V}{\partial P}\right)_T$ $(= 1/K_T$, see Equation 34) and the specific heat C_V (see Equation 28) are connected to each other through the following equation:

$$\alpha_V = \frac{\gamma C_V}{\beta_T V} \tag{36}$$

In order to compute γ in the lattice dynamic framework, we introduce the mode Grüneisen parameter $\gamma_s(\mathbf{q})$ and the specific heat $C_{V,s}(\mathbf{q})$ per phonon mode $\omega_s(\mathbf{q})$:

$$\gamma_s(\mathbf{q}) = -\frac{V}{\omega_s(\mathbf{q})}\left(\frac{\partial\omega_s(\mathbf{q})}{\partial V}\right)_T \tag{37}$$

$$C_{V,s}(\mathbf{q}) = k_B\left(\frac{\beta\hbar\omega_s(\mathbf{q})}{2\sinh(\frac{\beta\hbar\omega_s(\mathbf{q})}{2})}\right)^2 \tag{38}$$

It can be shown that the thermodynamic Grüneisen parameter γ is written :

$$\gamma = \frac{\sum_{s,\mathbf{q}}\gamma_s(\mathbf{q})C_{V,s}(\mathbf{q})}{C_V} \tag{39}$$

If the system undergoes an anisotropic strain $\epsilon_{\gamma\delta}$, such as $\sum_\kappa \epsilon_\kappa^2 = 1$ in the Voigt notation, the displacement of atom k becomes $\mathbf{u}_k^\gamma = \sum_\delta \epsilon_{\gamma\delta}\tau_k^\delta$. In this framework, the mode Grüneisen parameter rewrites [68] :

$$\gamma_s^{\gamma\delta}(\mathbf{q}) = -\frac{1}{3\omega_s(\mathbf{q})}\left(\frac{\partial\omega_s(\mathbf{q})}{\partial\epsilon_{\gamma\delta}}\right)_T = -\frac{1}{6\omega_s^2(\mathbf{q})}\left(\frac{\partial\omega_s^2(\mathbf{q})}{\partial\epsilon_{\gamma\delta}}\right)_T \tag{40}$$

Using Equations 22 and 21, we obtain :

$$\gamma_s^{\gamma\delta}(\mathbf{q}) = -\frac{1}{6\omega_s^2(\mathbf{q})}\frac{\partial}{\partial\epsilon_{\gamma\delta}}\left[\sum_{ij,\alpha\beta}X_{is}^{\star\alpha}(\mathbf{q})\sum_b\frac{1}{\sqrt{M_iM_j}}\frac{\partial^2 U}{\partial u_i^\alpha \partial u_j^\beta}\exp\left(i\mathbf{q}.\mathbf{R}(b)\right)X_{js}^\beta(\mathbf{q})\right] \tag{41}$$

In this equation one has to compute the third derivative with respect to displacements and strain. This one can be evaluated using the expansion of the Hamiltonian up to the third order:

$$\frac{\partial}{\partial\epsilon_{\gamma\delta}}\left(\frac{\partial^2 U}{\partial u_i^\alpha \partial u_j^\beta}\right) = \frac{\partial}{\partial\epsilon_{\gamma\delta}}\left(\overset{(2)}{\Theta}{}_{ij}^{\alpha\beta} + \sum_{k\gamma}\overset{(3)}{\Theta}{}_{ijk}^{\alpha\beta\gamma}u_k^\gamma\right) = \sum_k\overset{(3)}{\Theta}{}_{ijk}^{\alpha\beta\gamma}\tau_k^\delta \tag{42}$$

22

We obtain the common definition of the mode Grüneisen parameter as a function of the interatomic force constants.

$$\gamma_s^{\gamma\delta}(\mathbf{q}) = -\frac{1}{6\omega_s^2(\mathbf{q})} \sum_{ijk,bc,\alpha\beta} \overset{(3)}{\Theta}{}_{ijk}^{\alpha\beta\gamma}(0,b,c) \frac{X_{is}^{\star\alpha}(\mathbf{q})X_{js}^{\beta}(\mathbf{q})}{\sqrt{M_i M_j}} \tau_k^{\delta} \exp\left[i\mathbf{q}.\mathbf{R}(b)\right] \quad (43)$$

Once these parameters obtained, the thermodynamic Grüneisen parameter γ (see Equation 39) and the thermal expansion α_V (see Equation 36) can be computed directly. In the case of an anisotropic crystal, the thermal expansion matrix rewrites :

$$\alpha_V^{\alpha\beta} = \sum_{\gamma\delta} S_{\alpha\beta\gamma\delta} \sum_{\mathbf{q}s} C_{V,s}(\mathbf{q})\gamma_s^{\gamma\delta}(\mathbf{q}) \quad (44)$$

with $S_{\alpha\beta\gamma\delta} \equiv C_{\alpha\beta\gamma\delta}^{-1}$ the compliance matrix (see Equation 33). The volumetric thermal expansion α_V can be obtained by summing up the linear thermal expansion coefficients $\alpha_V^{\alpha\alpha}$ arranged along the diagonal of the thermal expansion matrix : $\alpha_V = \sum_i \alpha_V^{\alpha\alpha}$.

3.5. Thermal pressure, isentropic quantities, sound speed & Debye temperature

If the electronic entropy contribution is not considered, the total stress tensor can be split into two parts (see Equation 24) :

$$\sigma_{\alpha\beta} = \frac{1}{V}\left(\frac{\partial F}{\partial \epsilon_{\alpha\beta}}\right)_T = \sigma_{0,\alpha\beta} + \sigma_{\text{vib},\alpha\beta} \quad (45)$$

with the first part coming from the cold energy $U_0(V)$ and the second one being the thermal stress contribution deriving from the thermal free energy (see Equation 26) as :

$$\sigma_{\text{vib},\alpha\beta} = -\sum_{s,\mathbf{q}} \gamma_s^{\alpha\beta}(\mathbf{q})\frac{U_{\text{vib},s}(\mathbf{q})}{V} \quad \text{with} \quad (46)$$

$$U_{\text{vib},s}(\mathbf{q}) = \frac{\hbar\omega_s(\mathbf{q})}{2}\coth(\frac{\beta\hbar\omega_s(\mathbf{q})}{2}) \quad (47)$$

This result is really important since it becomes possible to verify that the pressure ($P = -\frac{1}{3}\text{Tr}[\sigma]$) computed using the AIMD code is well reproduced by the one computed using A-TDEP. The latter part involving the mode

Grüneisen parameter, it is a good way to check its convergence.

The thermodynamic Grüneisen parameter and the thermal expansion are also useful to compute the isentropic (or adiabatic) compressibility β_S and the constant-pressure heat capacity C_P:

$$
\begin{aligned}
\beta_S &= \beta_T(1 + \alpha_V \gamma T) = \frac{1}{K_S} & (48) \\
C_P &= C_V(1 + \alpha_V \gamma T) & (49)
\end{aligned}
$$

Note that β_T and C_V are already known (see Equations 34 and 28). Using the isentropic compressibility, the longitudinal v_l and transverse v_t sound speeds can be also obtained :

$$
v_l = \sqrt{\frac{K_S + 4G/3}{\rho}} \quad \text{and} \quad v_t = \sqrt{\frac{G}{\rho}} \tag{50}
$$

and the Debye temperature Θ_D becomes [69, 70] :

$$
\Theta_D = \frac{\hbar}{k_B}\left(6\pi^2 \frac{N_a}{V}\right)^{1/3} v_m \quad \text{with} \quad v_m = \left(\frac{1}{3}\left(\frac{2}{v_t^3} + \frac{1}{v_l^3}\right)\right)^{-1/3} \tag{51}
$$

4. a-TDEP inside the Abinit package

The algorithms and all the thermodynamic quantities detailed in the previous sections have been implemented in the ABINIT package. If the A-TDEP code is present in ABINIT since the Version 8.6 (released on November 3, 2017), the current described version is implemented in the Version 8.12.

As deeply integrated with ABINIT, it follows all its coding rules. It uses Fortran2003 language and makes use of data structures close to a Object-Oriented Programming. Thanks to the structures and features already implemented in ABINIT, many functionalities are directly taken from it for easiness, reliability and robustness. Regarding parallelism, even if ABINIT has several levels of parallelism [71] with both the Message Passing Interface (MPI) and OpenMP (threads), A-TDEP does not use parallelism yet. Nevertheless, compiling with a multithreaded linear algebra library will increase the performances of the code.

As A-TDEP takes place in the source tree of ABINIT, the build system of it is fully compatible and nothing more than the build system of ABINIT

is needed. Actually, during the configure step and build step of ABINIT, everything is set for A-TDEP. Therefore all the options and tuning of ABINIT can be used inside A-TDEP like tuning the linear algebra library and so on without any effort [72]. At the end of the build, a new executable is available (as ABINIT and many other post-process) and can be directly used.

For launching the executable, A-TDEP follows the same strategy as ABINIT. A *files* file can be provided (or a prompt will be displayed) containing :

1. The input file (`input.in`)

2. The molecular dynamic trajectory (the `_HIST.nc` file provided by ABINIT in the NETCDF format)

3. A root base name for all the output files (`root`).

Many output files are generated by the code, mainly for checking purpose. The main output file is :

1. `[root].out`. It includes an echo of the input variables, some intermediary results, the definition of the various shells of interaction, the IFC for all the atoms in each shell, the elastic constants and moduli, the energy of the model...

Other important files are also obtained :

2. `[root]omega.dat` contains the dispersion of phonon frequencies (in meV) along a path in the Brillouin Zone,

3. `[root]thermo.dat` lists all the thermodynamic quantities obtained by considering the system as a quantum harmonic crystal : specific heat, vibrational energy, entropy and free energy. It also gives all these contributions as a function of temperature in the harmonic approximation.

4. `[root]phonons-band.yaml` containing the phonon band structure in the PHONOPY convenient format [9]

5. `[root]sym.dat` details all the symmetry operations of the bravais lattice,

6. `[root]qpt.dat` defines the **q**-point grid used to compute the phonon frequencies contained in the `omega.dat` file,

7. `[root]xred_average.xyz` includes the ideal and average positions in the supercell,

8. `[root]Indym*.dat` contain all the symmetry relations between one or two atoms in the unitcell or the supercell,

9. `[root]vdos.dat` displays the vibrational density of states (in meV),

10. `[root]dij.dat` lists the dynamical matrices for a particular set of **q**-points,

11. `[root]etotMDvsTDEP[p].dat` compares the MD energies with the one computed using the pth order effective IFC as a function of time step (these ones must be superimposed, as much as possible) ,

12. `[root]fcartMDvsTDEP[p].dat` plots the MD forces wrt the forces computed using the pth order IFC (the cloud of points must be closer to the first bisector),

13. `[root]eigenvectors.dat` lists all the eigenvectors for a particular set of **q**-points,

14. `[root]nbcoeff-phij.dat/[root]nbcoeff-psij.dat` show how the number of IFC coefficients are reduced (for each shell and each symmetry) at the second and third order, respectively.

15. ...

For reliability and robustness, A-TDEP benefits from the full ABINIT test farm. ABINIT already includes more than 1200 tests that enables not only a strong guarantee on the results but also on portability of the code. A-TDEP takes advantages of all this pre-existent framework and includes its owns tests on several materials, geometry and physical quantities, including those presented in the following. This makes the code safer and more reliable.

To help the user, an external open source tool is also available. This one is called QTDEP and is interfaced with the present version of A-TDEP. Its use is very simple. First provide the set of configurations or molecular dynamic trajectory (first tab of Figure 2). After that, QTDEP will try to figure out what the unit cell is and if so, it will compute the multiplicity. If
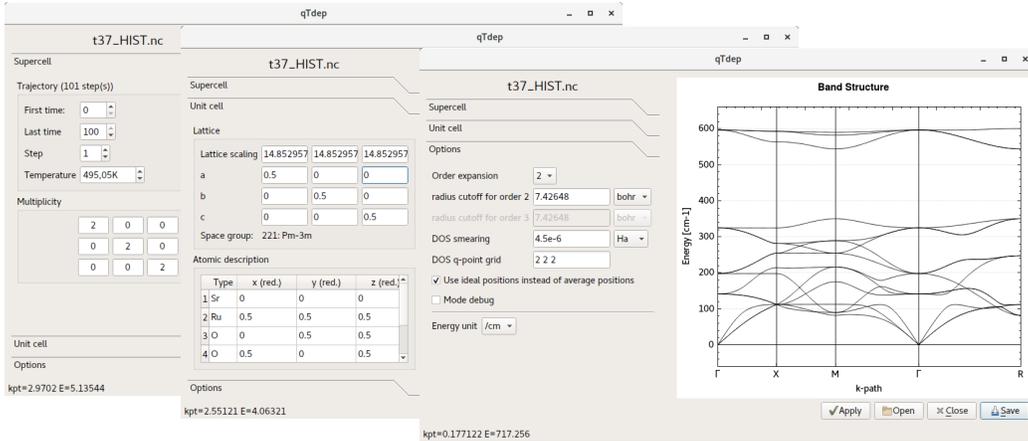
Figure 2: qTep GUI for A-TDEP. First tab is for the supercell and MD trajectory, second one for the reference structure (unitcell) and the last one is for some available options.

it can not determine it, the user has to provide an input file of this reference structure. Every time the unitcell is modified, the multiplicity of the supercell is recalculated. Finally, the last tabulation on Figure 2 shows the options available to perform the calculation. The order of the calculation (and thus the properties that can be extracted) the cutoff radius for each order and some boolean options to tweak the calculation. Then, when the changes are applied, the calculation is launched (A-TDEP has to be in the PATH environment variable) and when the calculation succeeds, the phonon dispersion curves are plotted. The input file for A-TDEP is created automatically by QTDEP so the user can change it by hand and tweak even more the calculation.

5. Examples illustrating the a-TDEP capabilities

In this section, we are interested in three materials : Si, Zr and U. The results provided below are not new or original. This section is just the occasion (*i*) to put into practice a large number of the A-TDEP capabilities (phonon frequencies, thermal expansion, Grüneisen parameters, elastic constants...) and (*ii*) to demonstrate that our home made implementation reproduce some results already published by Hellman and coworkers.
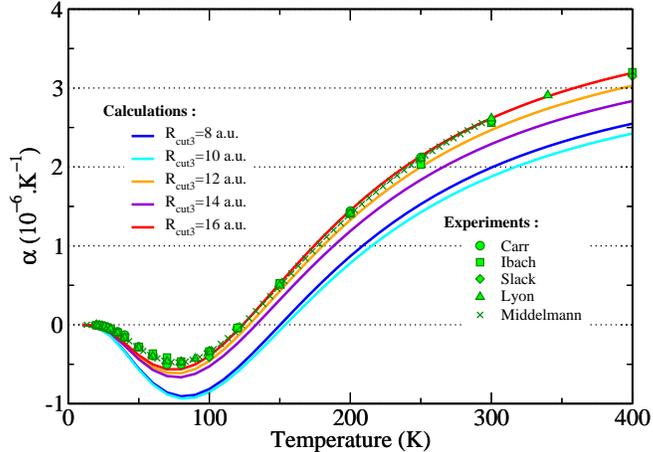
Figure 3: (Color online) Thermal expansion of silicon between 0 and 400 K. Experiments are from Carr *et al.* [73], Ibach *et al.* [74], Slack *et al.* [75], Lyon *et al.* [76] and Middelmann *et al.*[77].

5.1. Negative thermal expansion in silicon

The negative thermal expansion (NTE) of Si between 20 and 120 K (see Fig. 3) is a longstanding issue in condensed matter physics [78, 73, 74, 79, 75, 80, 76, 81, 82, 83, 84, 85, 86, 2, 45, 87, 30, 88, 77, 89]. If a good description of such unusual property can be provided in the framework of QHA [84, 89, 90], we will show in the following that a quantitative agreement is only recovered when thermal effects are explicitly taken into account, as shown by Kim *et al.*[90].

In order to compute accurate effective IFC by means of the least squares method, we have to accumulate a sufficiently large set of forces and positions. So, we perform AIMD simulations during 10 ps and select 250 configurations within (in the thermalized part of the trajectory). The supercell contains 216 atoms and the calculations are carried out in the NVT ensemble, at room temperature and using the experimental lattice parameter (a_{exp}=5.43 Å) rather than the theoretical one (a_{th}=5.40 Å).

Our calculations are performed by using the computational code ABINIT [91] over hundreds to thousands of processors [71]. A norm-conserving pseudopotential is generated following the Troullier-Martins scheme [92] in the

28

Kleinman-Bylander form [93], considering 4 electrons in the valence and a cutoff radius of 2.1 bohr leading to a cutoff energy equal to 380 eV. Exchange and correlation energy was treated with the local density approximation LDA using the Teter parametrization [94]. A careful treatment of the electronic density integration has been achieved with the use of a (2×2×2) Monkhorst-Pack mesh [95].

Two important parameters drive the number of IFC coefficients really computed during the A-TDEP calculation : R_{cut2} and R_{cut3}, the cutoff radii at the 2nd or 3rd order, respectively. We are tempted to put the highest possible value for these parameters. However, we face two limitations. The first one is the size of the supercell; the cutoff radius cannot exceed half of its lowest dimension. The second one is the computational cost : the larger these parameters, the greater the number of IFC coefficients to calculate. Therefore, five values has been used to check the convergence : 8, 10, 12, 14 and 16 a.u.. These cutoff radii lead to treat 6, 10, 16, 27 and 37 then 36, 95, 219, 711 and 1408 independent IFC coefficients, at the 2nd order and 3rd order respectively.

In Fig. 3, we display the variation of the linear thermal expansion α with respect to the temperature. In this figure, we compare the results obtained for the five values of the R_{cut3} parameter (with R_{cut2}=16 a.u.) with five sets of experimental data [73, 74, 75, 76, 77] (here, we do not consider the results of Batchelder and Simmons [78] since we find that there are inconsitent with the other experiments). As a function of the 3rd order cutoff, we obtain two groups of results : a poor agreement with experiments when the R_{cut3} parameter is "too low" (for 8 and 10 a.u.) and a better one when the R_{cut3} parameter is larger (for 12, 14 and 16 a.u.). At R_{cut3}=16 a.u., the agreement is surprisingly perfect, especially around the temperature used in the AIMD simulations (300 K), even if the convergence seems not completely achieved as a function of the cutoff radius. Our results are also in excellent agreement with the ones obtained using the original implementation of O. Hellman [90]. At higher temperature, the inclusion of the 4th order terms in the expansion of the energy (not considered here) are needed [58] to conserve a good agreement with experiments [90].

The convergence of the thermal expansion is in fact driven by the three quantities involved in its calculation : the thermodynamic Grüneisen parameter, the Bulk Modulus and the specific heat (see Equation 36). In Figure 4, we show the variation of the elastic constants C_{11}, C_{12} and the Bulk Modulus K_T as a function of the 2nd Order cutoff radius R_{cut2} (R_{cut3}=0 in this case).
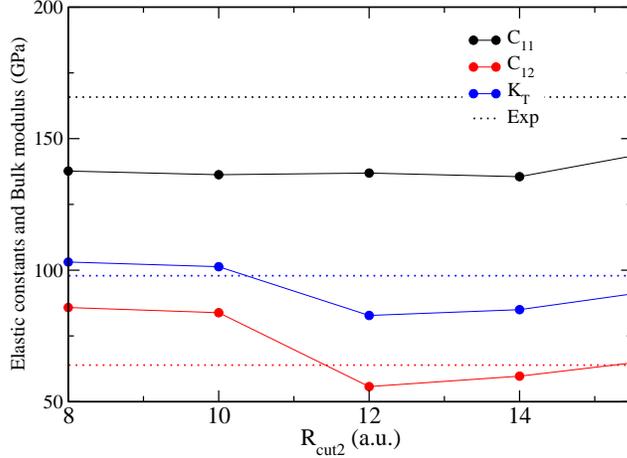
Figure 4: (Color online) Variation of the elastic constants of silicon C_{11} (black), C_{12} (red) and the Bulk Modulus K_T (blue) as a function of the 2nd Order cutoff radius R_{cut2}. For each, a dotted line with the same colour mentions the experimental value.

We see that the convergence of these three moduli is very long as a function of the cutoff radius, as already exposed for hcp Zr [67] or TiN [96]. Concerning the Bulk Modulus, the agreement with experiments is very good for R_{cut2}=8 or 10 a.u., due to an error compensation (negative error for C_{11} and positive error for C_{12}, see Eq. 34), then very bad for R_{cut2}=12 or 14 a.u. due to a better description of the C_{12}, and finally gives an intermediary value, with 7% of error wrt the experimental one.

Another important contribution to the thermal expansion is the thermodynamic Grüneisen parameter γ, built using the mode Grüneisen parameter $\gamma_s(\mathbf{q})$ (see Eq. 39). In Fig. 5, we can see a small variation in their dispersion curves when moving from the R_{cut3}=8 or 10 a.u. first group to the R_{cut3}=12, 14 or 16 a.u. second one. In all cases, the agreement with experiments [80] is very good. In the same time, this affects the thermodynamic Grüneisen parameter which goes from 0.34 (R_{cut3}=8 a.u.) to 0.42 (R_{cut3}=12 a.u.) and 0.45 (R_{cut3}=16 a.u.).

The third contribution to the thermal expansion is the specific heat $C_V(V,T)$, built using the phonon spectrum $\omega(V,T)$. As displayed in Fig. 6, the variation of the phonon dispersion curves as a function of the 2nd order

30
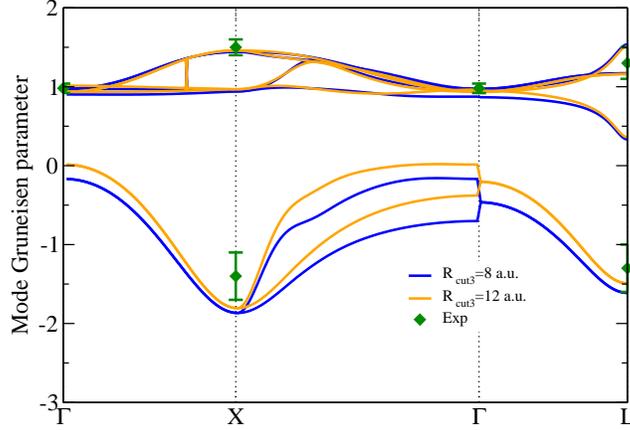
Figure 5: (Color online) Dispersion curves of the mode Grüneisen parameter of silicon computed using A-TDEP, for two cutoff radii (R_{cut3}=8 and 12 a.u.). The experimental data from Weinstein [80] are shown for comparison.
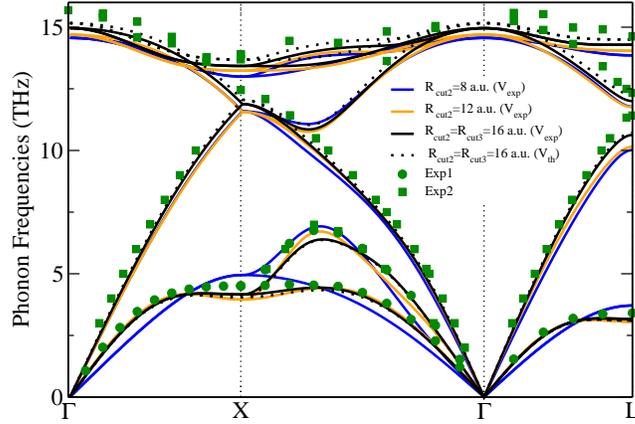
Figure 6: (Color online) Phonon spectra of silicon computed using A-TDEP for various values of 2nd and 3rd Order cutoff radii. The experimental data "Exp 1" are from Nilsson and Nelin [79] and "Exp 2" are from Kulda et al. [83].
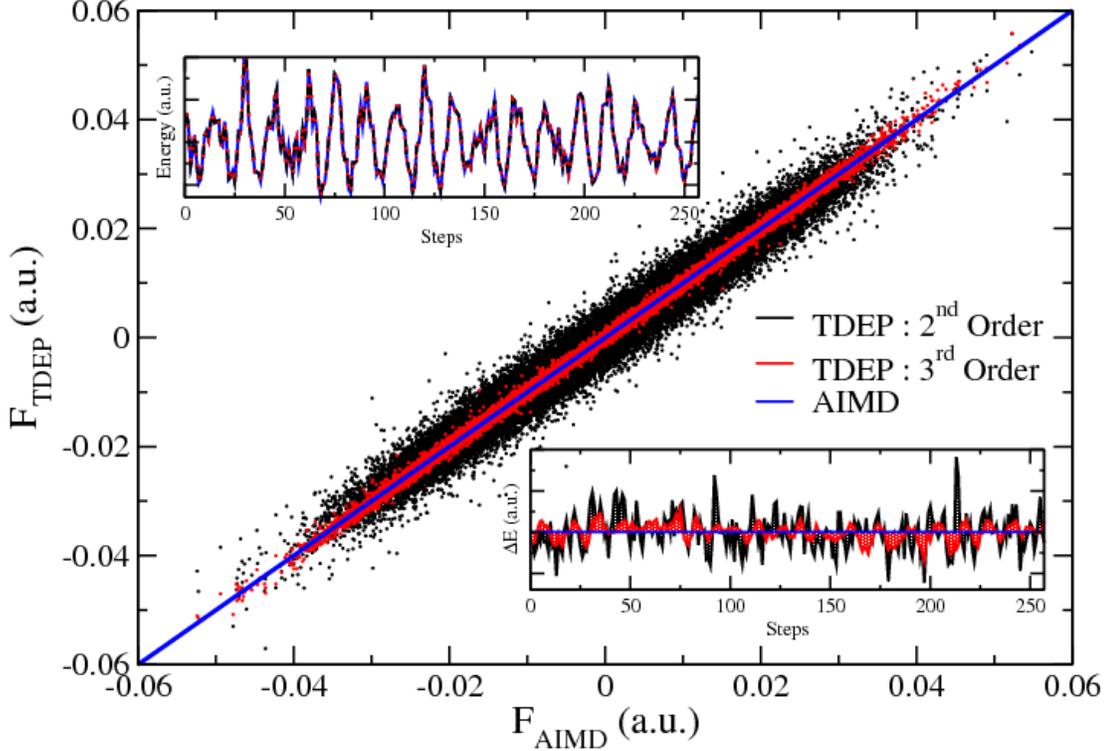
Figure 7: (Color online) Measure of the fit procedure : Forces of the model (TDEP) as a function of the AIMD ones for silicon. In the inset at the top left, we show the 2nd Order, 3rd Order and AIMD energies (they are all superimposed). In the inset at the bottom right, we show the energy differences (E^{2nd}_{TDEP}-E_{AIMD}) and (E^{3rd}_{TDEP}-E_{AIMD}).

cutoff radius is significant (in particular for the acoustic branches). Once again, two groups can be distinguished, according to the inclusion (or not) of the {100} shell in the A-TDEP calculation : a first group represented by the R_{cut2}=8 a.u. radius and a second one represented by the R_{cut2}=12 a.u. radius. For R_{cut2}=R_{cut3}=16 a.u., the agreement with experiments [79, 83] is excellent. Only the optical branches are slightly lower than experimental data (as also obtained by other authors before [30, 2]). The use of the theoretical lattice parameter rather than the experimental one slightly increases these optical branches, but it is not sufficient to have a perfect agreement.

At last, we present some very useful quantities which are available as outputs of A-TDEP and allow to check the fit procedure. After applying the least square method, the model (TDEP) has to reproduce correctly the

AIMD simulations. In Fig. 7, we plot the TDEP forces F_{TDEP} as a function of the AIMD ones F_{AIMD} and, in the two insets, the energies and their differences (for the 250 configurations selected at the beginning). We see clearly that the inclusion of the 3rd Order improves the fit. The standard deviation on forces goes from $\sigma=0.15$ at the 2nd Order to $\sigma=0.03$ at the 3rd Order. In addition, we can examine the variation of σ as a function of the 2nd Order cutoff radius. This one is equal to 0.166, 0.164, 0.152, 0.151 and 0.150 when the cutoff radius varies from 8 a.u. to 16 a.u.. The introduction of the $\{100\}$ shell reduces the standard deviation and leads to an improvement of the fit procedure.

In conclusion, an accurate description of the NTE in silicon can be achieved using A-TDEP, due to a good reproduction of its different parts (Bulk Modulus, thermodynamic Grüneisen parameter and specific heat). However, silicon does not show any strong variations of the phonon spectrum as a function of the temperature (in the [0 ; 400K] range). There is no (phase) stabilization or destabilization up to the melting. That is the reason why we show below two examples including explicit temperature effects that affect the phonon spectrum (and also the elasticity and the thermodynamic properties).

5.2. Thermal stabilization of the Zr bcc phase

In their original study, Hellman and coworkers [1] applied the TDEP method to the bcc phase of Zr. At 0 GPa, this structure is not stable at room temperature and all the calculations [98, 99] performed at 0 K show few soft modes in the phonon spectrum around the ω point (corresponding to $\mathbf{q} = (2/3, 2/3, 2/3)$ along the H-P high-symmetry line) and the Γ point.

In the present work, AIMD simulations are performed with 128 atoms in the supercell, using the NVT ensemble, for two temperatures (300 and 1000 K) and two pressures (around 0 and 30 GPa) during several ps. Our calculations are performed by using the ABINIT code [91] over hundreds to thousands of processors [71]. A projector augmented wave [100, 101] (PAW) atomic data is generated using the ATOMPAW code [102] in the XML format [103], considering 12 electrons in the valence and a cutoff radius of 2.2 bohr leading to a cutoff energy equal to 400 eV. Exchange and correlation energy was treated with the generalized gradient approximation (GGA) using the Perdew-Burke-Ernzerhof (PBE) functional [104]. As for Si, a careful treatment of the electronic density integration has been carried out with the use of a $(2\times2\times2)$ $\mathbf{k}$-point mesh.
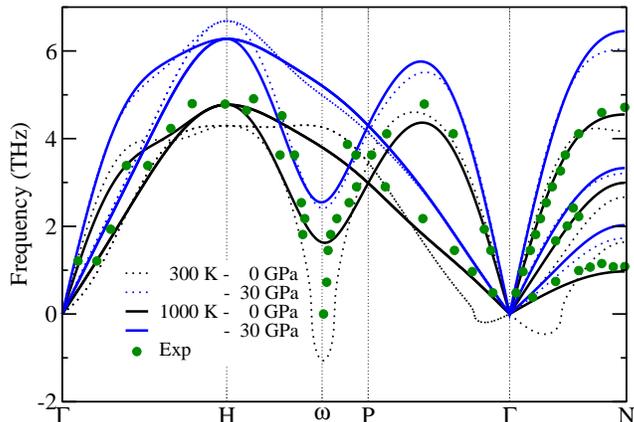
Figure 8: (Color online) Phonon spectra of bcc zirconium computed using A-TDEP at two temperatures (300 and 1000 K) and around two pressures (0 and 30 GPa). Experiment data come from Ref. [97].

In Fig. 8, we show the phonon spectra obtained by A-TDEP using only a 2nd order expansion of the energy, without any higher order terms. The soft modes disclosed by A-TDEP at 300 K (responsible for the instability) are suppressed when the temperature increases. In addition, we also notice that the phonon spectrum obtained at 1000 K is in very good agreement with experiments [97]. At last, we show in Fig. 8 the effect of pressure (30 GPa) on the phonon spectrum. In this case, the soft modes disappear which unveils the stabilization of the bcc phase at high pressure and room temperature, in line with experiments.

5.3. Failure of the QHA in α-U

Uranium is well-know to be the only element in the periodic table in which a charge density wave (CDW) state is observed at room pressure [105]. The phase transition at 50 K is accompanied by the softening of the longitudinal optic-like phonon mode in the [100] direction [106, 107, 108] and involves a doubling of the unit cell.

In the present work, AIMD simulations are performed with 96 atoms in a $4 \times 2 \times 3$ α-U supercell, using the NVT ensemble, for three temperatures (50,
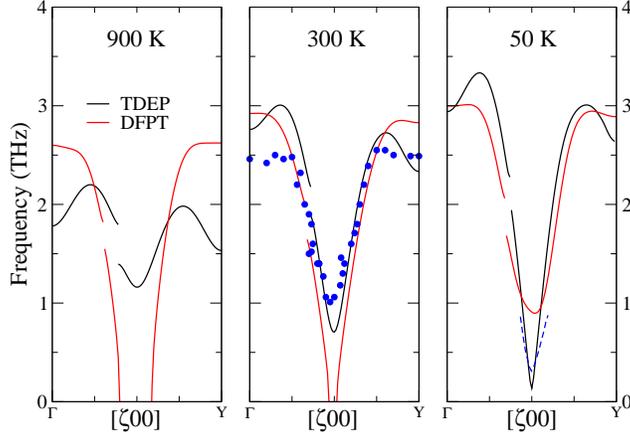
Figure 9: (Color online) Phonon frequencies of the longitudinal optic-like mode of α-U at 900, 300 and 50 K. Black lines : A-TDEP, red lines : DFPT. Experimental neutron-scattering data [106] at room temperature are denoted by blue circles and by the dashed line at 30 K [107].

300 and 900 K) during several ps. Our calculations are performed by using the ABINIT code [91] over hundreds to thousands of processors [71]. A PAW [100, 101] atomic data is generated using the ATOMPAW code [102] in the XML format [103], considering 14 electrons in the valence and a cutoff radius of 2.85 bohr leading to a cutoff energy equal to 435 eV. Exchange and correlation energy was treated using the GGA-PBE functional [104].

In Fig. 9, we compare the temperature dependence of the longitudinal optic-like phonon mode obtained using the DFPT (at 0 K), with A-TDEP at 50, 300 and 900 K (using only a 2nd order expansion of the energy, without any higher order terms) with experimental data at 50 and 300 K. We use the experimental lattice parameter at each temperature for both methods (for more computational details, please see Ref. [50]).

With A-TDEP we capture the softening of the phonon mode. At 900 K the α-U structure is stable and as the temperature decreases from 900 to 50 K the phonon branch strongly softens with a well pronounced dip located near $\mathbf{q} = (1/2, 0, 0)$ along the $[\zeta 00]$ high-symmetry line. The frequencies are in excellent agreement with neutron-scattering data at 300 and 30 K [106, 107].

35

On the other hand, the results obtained with DFPT in QHA are in contradiction with the experimental observations. The α-U structure is predicted to be unstable at volumes corresponding to 900 and 300 K, due to imaginary frequencies. By contrast, it becomes stable at volume corresponding to 50 K when the phase transition towards the CDW state takes place. This example clearly highlight the failure of the QHA when explicit temperature effects are present.

Conclusion

We have developed a post process code able to handle the anharmonic effects. This one is based on the TDEP method and is distributed in the ABINIT code under the GNU-GPL license. Many features can be computed using A-TDEP : phonon spectrum, elastic constants and moduli, Grüneisen parameters, thermal expansion, free energies... These capabilities have been checked on many materials (Si, U [50, 52], Zr, Pu [53], MgO [55], Ti [51], Fe [54]), in various thermodynamic situations (low/high temperature/pressure), and excellent agreements with experimental data are obtained everytime.

This paper paves the way to have a complete reference support for the user of A-TDEP. It includes the theory needed to understand the TDEP method and to compute thermodynamic quantities, the algorithms used in this A-TDEP implementation, numerous references to works applying this method but also to other similar approaches and finally, several examples showing the capabilities of this code.

The choice to implement the A-TDEP code in ABINIT is definitively valuable since this post-process actually benefits of all the developments from the ABINIT ecosystem : the symmetries coming from the lattice or magnetic space group, the treatment of the dipole-dipole interaction [10], the input-output file formats (NETCDF, YAML...), the definition of Monkhorst-Pack grids of $\mathbf{q}$-points used to computed the vDOS or other thermodynamic quantities, the stochastic generation of thermalized configurations [90]... In the future, other interplay are expected, in particular the use of A-TDEP during the execution of ABINIT or MULTIBINIT [109].

The present version of the A-TDEP code does not include several features. In particular, the 4th order is not implemented [57, 58, 59], so the phonon lifetime, the frequency shift, the thermal conductivity, the spectral function and the anharmonic corrections to thermodynamic (free energy, heat

capacity...) and elastic (sound speed, Grüneisen parameter...) quantities will be available in the next version.

Acknowledgments

References

[1] O. Hellman, I. Abrikosov, S. Simak, Lattice dynamics of anharmonic solids from first principles, Phys. Rev. B 84 (2011) 180301(R).

[2] K. Esfarjani, H. T. Stokes, Method to extract anharmonic force constants from first principles calculations, Phys. Rev. B 77 (2008) 144112.

[3] The present results have been obtained through the use of the ABINIT code, a common project of the Université Catholique de Louvain, Corning Incorporated, and other contributors, see the URL http://www.abinit.org.

[4] O. L. Anderson, The grüneisen ratio for the last 30 years, Geophysical Journal International 143 (2) (2000) 279–294. arXiv:https://onlinelibrary.wiley.com/doi/pdf/10.1046/j.1365-246X.2000.01266.x, doi:10.1046/j.1365-246X.2000.01266.x. URL https://onlinelibrary.wiley.com/doi/abs/10.1046/j.1365-246X.2000.01266.x

[5] G. Lucazeau, Effect of pressure and temperature on raman spectra of solids: anharmonicity, Journal of Raman Spectroscopy 34 (7-8) (2003) 478–496. arXiv:https://onlinelibrary.wiley.com/doi/pdf/10.1002/jrs.1027, doi:10.1002/jrs.1027. URL https://onlinelibrary.wiley.com/doi/abs/10.1002/jrs.1027

[6] W. Holzapfel, Effects of intrinsic anharmonicity in the mie-grüneisen equation of state and higher order corrections, High Pressure Res. 25 (2005) 187.

[7] S. d'Ambrumenil, M. Zbiri, A. M. Chippindale, S. J. Hibble, E. Marelli, A. C. Hannon, Lattice dynamics and negative thermal expansion in the framework compound $ZnNi(CN)_4$ with two-dimensional and three-dimensional local environments, Phys. Rev. B 99 (2019) 024309. doi:10.1103/PhysRevB.99.024309.
URL https://link.aps.org/doi/10.1103/PhysRevB.99.024309

[8] K. Parlinski, Z. Li, Y. Kawazoe, First-principle determination of the soft mode in cubic zro_2, Phys. Rev. B 78 (1997) 4064.

[9] A. Togo, F. Oba, I. Tanaka, First-principles calculations of the ferroelastic transition between rutile-type and $cacl_2$-type sio_2 at high pressure, Phys. Rev. B 78 (2008) 134106.

[10] X. Gonze, C. Lee, Dynamical matrices, born effectives charges, dielectric permittivity tensors, and interatomic force constants from density-functional perturbation theory, Phys. Rev. B 55 (1997) 10355.

[11] S. Baroni, S. de Gironcoli, A. D. Corso, P. Giannozzi, Phonons and related crystal properties from density-functional perturbation theory, Rev. Mod. Phys. 73 (1997) 515.

[12] T. Feng, X. Ruan, Quantum mechanical prediction of four-phonon scattering rates and reduced thermal conductivity of solids, Phys. Rev. B 93 (2016) 045202. doi:10.1103/PhysRevB.93.045202.
URL https://link.aps.org/doi/10.1103/PhysRevB.93.045202

[13] T. Tadano, S. Tsuneyuki, First-principles lattice dynamics method for strongly anharmonic crystals, J. Phys. Soc. Jpn. 87 (2018) 041015.

[14] L. Paulatto, F. Mauri, M. Lazzeri, Anharmonic properties from a generalized third-order ab initio approach: Theory and applications to graphite and graphene, Phys. Rev. B 87 (2013) 214303. doi:10.1103/PhysRevB.87.214303.
URL https://link.aps.org/doi/10.1103/PhysRevB.87.214303

[15] X. Gonze, J.-P. Vigneron, Density-functional approach to nonlinear-response coefficients of solids, Phys. Rev. B 39 (1989) 13120–13128. doi:10.1103/PhysRevB.39.13120.
URL https://link.aps.org/doi/10.1103/PhysRevB.39.13120

[16] G. Leibfried, W. Ludwig, Solid State Physics Vol 12 : Theory of anharmonic Effects in Crystals, Academic Press, New York, 1961, pp. 275–444.

[17] A. A. Maradudin, A. E. Fein, Scattering of neutrons by anharmonic crystal, Phys. Rev. 128 (1962) 2589.

[18] R. Cowley, Anharmonics crystals, Rep. Prog. Phys. 31 (1968) 123.

[19] T. Barron, M. Klein, Dynamical properties of solids : Volume 1. Crystalline Solids, fundamentals, North Holland, Amsterdam, 1974, p. 391.

[20] P. Brüesch, Phonons : Theory and Experiments I, Springer-Verlag, Berlin Heidelberg, 1982.

[21] D. C. Wallace, Thermodynamics of Crystals, Dover, New York, 1997.

[22] D. C. Wallace, Statistical physics of crystals and liquids, World Scientific Publishing Company, Singapore, 2003.

[23] P. Souvatzis, O. Eriksson, M. I. Katsnelson, S. P. Rudin, Entropy driven stabilization of energetically unstable crystal structures explained from first principles theory, Phys. Rev. Lett. 100 (2008) 095901.

[24] P. Souvatzis, S. Rudin, Dynamical stabilization of cubic zro_2 by phonon-phonon interactions: Ab initio calculations, Phys. Rev. B 78 (2008) 184304.

[25] P. Souvatzis, O. Eriksson, M. I. Katsnelson, S. P. Rudin, The self-consistent ab initio lattice dynamical method, Comp. Mater. Sci. 44 (2009) 888.

[26] W. Luo, B. Johansson, O. Eriksson, S. Arpan, P. Souvatzis, M. I. Katsnelson, R. Ahuja, Dynamical stability of body center cubic iron at the earths core conditions, PNAS 107 (2010) 9962.

[27] A. Togo, I. Tanaka, First principles phonon calculations in materials science, Scr. Mater. 108 (2015) 1.

[28] J. Linnera, A. J. Karttunen, Ab initio study of the lattice thermal conductivity of cu_2o using the generalized gradient approximation and hybrid functional methods, Phys. Rev. B 96 (2017) 014304.

[29] A. Carreras, A. Togo, I. Tanaka, Dynaphopy : A code for extracting phonon quasiparticles from molecular dynamics simulations, Comp. Phys. Comm. 221 (2017) 221.

[30] T. Tadano, Y. Gohda, S. Tsuneyuki, Anharmonic force constants extracted from first-principles molecular dynamics: applications to heat transfer simulations, J. Phys. Condens. Matter 26 (2014) 225012.

[31] T. Tadano, S. Tsuneyuki, Self-consistent phonon calculations of lattice dynamical properties in cubic srtio$_3$ with first-principles anharmonic force constants, Phys. Rev. B 92 (2015) 054301.

[32] T. Tadano, Y. Gohda, S. Tsuneyuki, Impact of rattlers on thermal conductivity of a thermoelectric clathrate: A first-principles study, Phys. Rev. Lett. 114 (2016) 095501.

[33] I. Errea, M. Calandra, F. Mauri, First-principles theory of anharmonicity and the inverse isotope effect in superconducting palladium-hydride compounds, Phys. Rev. Lett. 111 (2013) 177002.

[34] I. Errea, M. Calandra, F. Mauri, Anharmonic free energies and phonon dispersions from the stochastic self-consistent harmonic approximation: Application to platinum and palladium hydrides, Phys. Rev. B 89 (2014) 064302.

[35] L. Paulatto, I. Errea, M. Calandra, F. Mauri, First-principles calculations of phonon frequencies, lifetimes, and spectral functions from weak to strong anharmonicity: The example of palladium hydrides, Phys. Rev. B 91 (2015) 054304.

[36] M. Borinaga, I. Errea, M. Calandra, F. Mauri, A. Bergara, Anharmonic effects in atomic hydrogen: Superconductivity and lattice dynamical stability, Phys. Rev. B 93 (2016) 174308.

[37] R. Bianco, I. Errea, L. Paulatto, M. Calandra, F. Mauri, Second-order structural phase transitions, free energy curvature, and temperature-dependent anharmonic phonons in the self-consistent harmonic approximation : Theory and stochastic implementation, Phys. Rev. B 96 (2017) 014111.

[38] L. J. Nelson, G. L. W. Hart, F. Zhou, V. Ozolins, Compressive sensing as a paradigm for building physics models, Phys. Rev. B 87 (2013) 035125.

[39] F. Zhou, W. Nielson, Y. Xia, V. Ozolins, Lattice anharmonicity and thermal conductivity from compressive sensing of first-principles calculations, Phys. Rev. Lett. 113 (2014) 185501.

[40] A. Glensk, B. Grabowski, T. Hickel, J. Neugebauer, Breakdown of the arrhenius law in describing vacancy formation energies: The importance of local anharmonicity revealed by ab initio thermodynamics, Phys. Rev. X 4 (2014) 011018.

[41] A. Glensk, B. Grabowski, T. Hickel, J. Neugebauer, Understanding anharmonicity in fcc materials: From its origin to ab initio strategies beyond the quasiharmonic approximation, Phys. Rev. Lett. 114 (2015) 195901.

[42] A. I. Duff, T. Davey, D. Korbmacher, A. Glensk, B. Grabowski, J. Neugebauer, M. W. Finnis, Improved method of calculating ab initio high-temperature thermodynamic properties with application to zrc, Phys. Rev. B 91 (2015) 214311.

[43] C. Toher, J. J. Plata, O. Levy, M. de Jong, M. Asta, M. B. Nardelli, S. Curtarolo, High-throughpout computational screening of thermal conductivity, debye temperature, and grüneisen parameters using a quasiharmonic debye model, Phys. Rev. B 90 (2014) 174107.

[44] J. J. Plata, P. Nath, D. Usanmaz, J. C. C. Toher, M. de Jong, M. Asta, M. Fornari, M. B. Nardelli, S. Curtarolo, An efficient and accurate framework for calculating lattice thermal conductivity of solids : Aflow–appl automatic anharmonic phonon library, Computational Materials 45 (2017) 1.

[45] K. Esfarjani, G. Chen, H. T. Stokes, Heat transport in silicon from first-principles calculations, Phys. Rev. B 84 (2011) 085204.

[46] J. Shiomi, K. Esfarjani, G. Chen, Thermal conductivity of half-heusler compounds from first-principles calculations, Phys. Rev. B 84 (2011) 085204.

[47] O. Hellman, P. Steneteg, I. Abrikosov, S. Simak, Temperature dependent effective potential method for accurate free energy calculations of solids, Phys. Rev. B 87 (2013) 104111.

[48] O. Hellman, I. Abrikosov, Temperature-dependent effective third-order interatomic force constants from first principles, Phys. Rev. B 88 (2013) 144301.

[49] N. Shulumba, O. Hellman, A. J. Minnich, Lattice thermal conductivity of polyethylene molecular crystals from first-principles including nuclear quantum effects, Phys. Rev. Lett. 119 (2017) 185901.

[50] J. Bouchet, F. Bottin, Thermal evolution of vibrational properties of α-u, Phys. Rev. B 92 (2015) 174108.

[51] A. Dewaele, V. Stutzmann, J. Bouchet, F. Bottin, F. Occelli, M. Mezouar, High pressure-temperature phase diagram and equation of state of titanium, Phys. Rev. B 91 (2015) 134108.

[52] J. Bouchet, F. Bottin, High-temperature and high-pressure phase transitions in uranium, Phys. Rev. B 95 (2017) 054113.

[53] B. Dorado, F. Bottin, J. Bouchet, Phonon spectra of plutonium at high temperatures, Phys. Rev. B 95 (2017) 104303.

[54] A. Dewaele, V. Svitlyk, F. Bottin, J. Bouchet, J. Jacobs, Iron under conditions close to the $\alpha - \gamma - \epsilon$ triple point, Applied Physics Letters 112 (20) (2018) 201906. arXiv:https://doi.org/10.1063/1.5030192, doi:10.1063/1.5030192.
URL https://doi.org/10.1063/1.5030192

[55] J. Bouchet, F. Bottin, V. Recoules, F. Remus, G. Morard, R. M. Bolis, A. Benuzzi-Mounaix, Ab initio calculations of the B1-B2 phase transition in MgO, Phys. Rev. B 99 (2019) 094113.

[56] X. Gonze, J.-M. Beuken, R. Caracas, F. Detraux, M. Fuchs, G.-M. Rignanese, L. Sindic, M. Verstraete, G. Zerah, F. Jollet, M. Torrent, A. Roy, M. Mikami, P. Ghosez, J.-Y. Raty, D. Allan, First-principles computation of material properties: the abinit software project, Comput. Mater. Sci 25 (2002) 478.

[57] T. Feng, L. Lindsay, X. Ruan, Four-phonon scattering significantly reduces intrinsic thermal conductivity of solids, Phys. Rev. B 96 (2017) 161201.

[58] S.-Y. Yue, X. Zhang, G. Qin, S. R. Phillpot, M. Hu, Metric for strong intrinsic fourth-order phonon anharmonicity, Phys. Rev. B 95 (2017) 195203.

[59] N. K. Ravichandran, Unified first-principles theory of thermal properties of insulators, Phys. Rev. B 98 (2018) 085205.

[60] C. Lee, X. Gonze, Ab initio calculation of the thermodynamic properties and atomic temperature factors of sio_2 α-quartz and stishovite, Phys. Rev. B 51 (1995) 8610.

[61] T. H. K. Barron, M. L. Klein, Thermal and elastic properties of crystals at low temperatures, Phys. Rev. 127 (1962) 1997–1998. doi:10.1103/PhysRev.127.1997.
URL https://link.aps.org/doi/10.1103/PhysRev.127.1997

[62] R. Cowley, Zero sound, first sound and second sound of solids, Proc. Phys. Soc. 90 (1967) 1127.

[63] R. C. Shukla, H. Hübschle, Atomic mean-square displacement of a solid : A green's-function approach, Phys. Rev. B 40 (1989) 1556.

[64] P. B. Allen, Anharmonic phonon quasiparticle theory of zero-point and thermal shifts in insulators: Heat capacity, bulk modulus, and thermal expansion, Phys. Rev. B 92 (2015) 064106. doi:10.1103/PhysRevB.92.064106.
URL https://link.aps.org/doi/10.1103/PhysRevB.92.064106

[65] Y. Oba, T. Tadano, R. Akashi, S. Tsuneyuki, First-principles study of phonon anharmonicity and negative thermal expansion in scf_3, Phys. Rev. Materials 3 (2019) 033601. doi:10.1103/PhysRevMaterials.3.033601.
URL https://link.aps.org/doi/10.1103/PhysRevMaterials.3.033601

[66] D. V. Minakov, P. R. Levashov, Melting curves of metals with excited electrons in the quasiharmonic approximation, Phys. Rev. B 92 (2015)

224102. doi:10.1103/PhysRevB.92.224102.
URL https://link.aps.org/doi/10.1103/PhysRevB.92.224102

[67] I. Schnell, M. Jones, S. Rudin, R. Albers, Tight-binding calculations of the elastic constants and phonons of hcp zr: Complications due to anisotropic stress and long-range forces, Phys. Rev. B 74 (2006) 054104.

[68] C. H. Lee, C. K. Gan, Anharmonic interatomic force constants and thermal conductivity from grüneisen parameters : An application to graphene, Phys. Rev. B 96 (2017) 035105.

[69] H. Shao, X. Tan, J. Jiang, H. Jiang, First-principles study on the elastic properties of cu2gese3, EPL (Europhysics Letters) 113 (2) (2016) 26001. doi:10.1209/0295-5075/113/26001.
URL https://doi.org/10.1209

[70] N. Ashcroft, N. Mermin, Solid State Physics, Saunders College, Philadelphia, 1976.

[71] F. Bottin, S. Leroux, A. Knyazev, G. Zérah, Large-scale *ab initio* calculations based on three levels of parallelization, Comput. Mater. Sci. 42 (2) (2008) 329.

[72] X. Gonze, *et al.*, Abinit: First-principles approach to material and nanosystem properties, Computer Physics Communications XXX (2019) YYY.

[73] R. Carr, R. McCammon, G. White, Thermal expansion of germanium and silicon at low temperatures, Phil. Mag. 12 (1965) 157.

[74] H. Ibach, Thermal expansion of silicon and zinc oxide (i), Phys. Status Solidi B 31 (1969) 625.

[75] G. A. Slack, S. F. Bartram, Thermal expansion of some diamondlike crystals, Journal of Applied Physics 46 (1) (1975) 89–98. arXiv:https://doi.org/10.1063/1.321373, doi:10.1063/1.321373.
URL https://doi.org/10.1063/1.321373

[76] K. G. Lyon, G. L. Salinger, C. A. Swenson, G. K. White, Linear thermal expansion measurements on silicon from 6 to 340 k., Journal of Applied Physics 48 (3) (1977) 865–868.

arXiv:https://doi.org/10.1063/1.323747, doi:10.1063/1.323747.
URL https://doi.org/10.1063/1.323747

[77] T. Middelmann, A. Walkov, G. Bartl, R. Schödel, Thermal expansion coefficient of single-crystal silicon from 7 k to 293 k, Phys. Rev. B 92 (2015) 174113. doi:10.1103/PhysRevB.92.174113.
URL https://link.aps.org/doi/10.1103/PhysRevB.92.174113

[78] D. N. Batchelder, R. O. Simmons, Lattice constants and thermal expansivities of silicon and of calcium fluoride between 6^{deg} and 322^{deg}k, The Journal of Chemical Physics 41 (8) (1964) 2324–2329. arXiv:https://doi.org/10.1063/1.1726266, doi:10.1063/1.1726266.
URL https://doi.org/10.1063/1.1726266

[79] G. Nilsson, G. Nelin, Study of the homology between silicon and germanium by thermal-neutron spectrometry, Phys. Rev. B 6 (1972) 3777–3786. doi:10.1103/PhysRevB.6.3777.
URL https://link.aps.org/doi/10.1103/PhysRevB.6.3777

[80] B. A. Weinstein, G. J. Piermarini, Raman scattering and phonon dispersion in si and gap at very high pressure, Phys. Rev. B 12 (1975) 1172.

[81] Y. Okada, Y. Tokumaru, Precise determination of lattice parameter and thermal expansion coefficient of silicon between 300 and 1500 k, Journal of Applied Physics 56 (2) (1984) 314–320. arXiv:https://doi.org/10.1063/1.333965, doi:10.1063/1.333965.
URL https://doi.org/10.1063/1.333965

[82] D. Strauch, A. P. Mayer, B. Dorner, Phonon eigenvectors in si determined by inelastic neutron scattering, Zeitschrift für Physik B Condensed Matter 78 (3) (1990) 405–410. doi:10.1007/BF01313321.
URL https://doi.org/10.1007/BF01313321

[83] J. c. v. Kulda, D. Strauch, P. Pavone, Y. Ishii, Inelastic-neutron-scattering study of phonon eigenvectors and frequencies in si, Phys. Rev. B 50 (1994) 13347–13354. doi:10.1103/PhysRevB.50.13347.
URL https://link.aps.org/doi/10.1103/PhysRevB.50.13347

[84] G.-M. Rignanese, J. Michenaud, X. Gonze, Ab initio study of the volume dependence of dynamical and thermodynamical propoerties of silicon, Phys. Rev. B 53 (1996) 4488.

[85] J. Fabian, P. B. Allen, Thermal expansion and grüneisen parameters of amorphous silicon: A realistic model calculation, Phys. Rev. Lett. 79 (1997) 1885–1888. doi:10.1103/PhysRevLett.79.1885.
URL https://link.aps.org/doi/10.1103/PhysRevLett.79.1885

[86] D. Broido, A. Ward, N. Mingo, Lattice thermal conductivity of silicon from thermal interatomic potentials, Phys. Rev. B 72 (2005) 014308.

[87] V. J. Härkonen, A. J. Karttunen, Ab initio lattice dynamical studies of silicon clathrate frameworks and their negative thermal expansion, Phys. Rev. B 89 (2014) 024305.

[88] D. Kim, H. Smith, J. Niedziela, C. Li, D. Abernathy, B. Fultz, Phonon anharmonicity in silicon from 100 to 1500 k, Phys. Rev. B 91 (2015) 014307.

[89] U. Argaman, E. Eidelstein, O. Levy, G. Makov, Ab initio study of the phononic origin of negative thermal expansion, Phys. Rev. B 94 (2016) 174305.

[90] D. S. Kim, O. Hellman, J. Herriman, H. L. Smith, J. Y. Y. Lin, N. Shulumba, J. L. Niedziela, C. W. Li, D. L. Abernathy, B. Fultz, Nuclear quantum effect with pure anharmonicity and the anomalous thermal expansion of silicon, Proceedings of the National Academy of Sciences 115 (9) (2018) 1992–1997. arXiv:https://www.pnas.org/content/115/9/1992.full.pdf, doi:10.1073/pnas.1707745115.
URL https://www.pnas.org/content/115/9/1992

[91] X. Gonze, B. Amadon, P.-M. Anglade, J.-M. Beuken, F. Bottin, P. Boulanger, F. Bruneval, D. Caliste, R. Caracas, M. Côté, T. Deutsch, L. Genovese, P. Ghosez, M. Giantomassi, S. Goedecker, D. Hamann, P. Hermet, F. Jollet, G. Jomard, S. Leroux, M. Mancini, S. Mazevet, M. Oliveira, G. Onida, Y. Pouillon, T. Rangel, G.-M. Rignanese, D. Sangalli, R. Shaltaf, M. Torrent, M. Verstraete, G. Zerah, J. Zwanziger, Abinit: First-principles approach to material and

nanosystem properties, Computer Physics Communications 180 (12) (2009) 2582–2615, 40 YEARS OF CPC: A celebratory issue focused on quality software for high performance, grid and novel computing architectures. doi:DOI: 10.1016/j.cpc.2009.07.007.
URL http://www.sciencedirect.com/science/article/B6TJ5-4WTRSCM-3/2/20edf8da7(

[92] N. Troullier, J. L. Martins, Efficient pseudopotentials for plane-wave calculations, Phys. Rev. B 43 (1991) 1993.

[93] L. Kleinman, D. M. Bylander, Efficacious form for model pseudopotentials, Phys. Rev. Lett. 48 (1982) 1425.

[94] S. Goedecker, M. Teter, J. Hutter, Separable dual-space gaussian pseudopotentials, Phys. Rev. B 54 (1996) 1703.

[95] H. J. Monkhorst, J. D. Pack, Special points for brillouin-zone integrations, Phys. Rev. B 13 (1976) 5188.

[96] P. Steneteg, O. Hellman, O. Y. Vekilova, N. Shulumba, F. Tasnádi, I. A. Abrikosov, Temperature dependence of tin elastic constants from ab initio molecular dynamics simulations, Phys. Rev. B 87 (2013) 094114. doi:10.1103/PhysRevB.87.094114.
URL https://link.aps.org/doi/10.1103/PhysRevB.87.094114

[97] A. Heiming, W. Petry, J. Trampenau, M. Alba, C. Herzig, H. R. Schober, G. Vogl, Phonon dispersion of the bcc phase of group-iv metals. ii. bcc zirconium, a model case of dynamical precursors of martensitic transitions, Phys. Rev. B 43 (1991) 10948–10962. doi:10.1103/PhysRevB.43.10948.
URL https://link.aps.org/doi/10.1103/PhysRevB.43.10948

[98] B.-T. Wang, P. Zhang, H.-Y. Liu, W.-D. Li, P. Zhang, First-principles calculations of phase transition, elastic modulus, and superconductivity under pressure for zirconium, Journal of Applied Physics 109 (6) (2011) 063514. arXiv:https://doi.org/10.1063/1.3556753, doi:10.1063/1.3556753.
URL https://doi.org/10.1063/1.3556753

[99] X. Qian, R. Yang, Temperature effect on the phonon dispersion stability of zirconium by machine learning driven atomistic simulations,

Phys. Rev. B 98 (2018) 224108. doi:10.1103/PhysRevB.98.224108.
URL https://link.aps.org/doi/10.1103/PhysRevB.98.224108

[100] P. E. Blöchl, Projector augmented-wave method, Phys. Rev. B 50 (1994) 17953.

[101] M. Torrent, F. Jollet, F. Bottin, G. Zérah, X. Gonze, Implementation of the projector augmented-wave method in the abinit code: Application to the study of iron under pressure, Comput. Mater. Sci. 42 (2) (2008) 337.

[102] N. Holzwarth, A. Tackett, G. Matthews, A projector augmented wave (paw) code for electronic structure calculations, part i: atompaw for generating atom-centered functions, Computer Physics Communications 135 (3) (2001) 329 – 347. doi:https://doi.org/10.1016/S0010-4655(00)00244-7.
URL http://www.sciencedirect.com/science/article/pii/S0010465500002447

[103] F. Jollet, M. Torrent, N. Holzwarth, Generation of projector augmented-wave atomic data: A 71 element validated table in the xml format, Computer Physics Communications 185 (4) (2014) 1246 – 1254. doi:https://doi.org/10.1016/j.cpc.2013.12.023.
URL http://www.sciencedirect.com/science/article/pii/S0010465513004359

[104] J. P. Perdew, K. Burke, M. Ernzerhof, Generalized gradient approximation made simple, Phys. Rev. Lett. 77 (1996) 3865.

[105] G. Lander, E. Fisher, S. Bader, The solid-state properties of uranium a historical perspective and review, Advances in Physics 43 (1) (1994) 1–111. arXiv:https://doi.org/10.1080/00018739400101465, doi:10.1080/00018739400101465.
URL https://doi.org/10.1080/00018739400101465

[106] W. P. Crummett, H. G. Smith, R. M. Nicklow, N. Wakabayashi, Lattice dynamics of α-uranium, Phys. Rev. B 19 (1979) 6028–6037. doi:10.1103/PhysRevB.19.6028.
URL https://link.aps.org/doi/10.1103/PhysRevB.19.6028

[107] H. G. Smith, N. Wakabayashi, W. P. Crummett, R. M. Nicklow, G. H. Lander, E. S. Fisher, Observation of a charge-density wave

in α-u at low temperature, Phys. Rev. Lett. 44 (1980) 1612–1615. doi:10.1103/PhysRevLett.44.1612.
URL `https://link.aps.org/doi/10.1103/PhysRevLett.44.1612`

[108] J. Bouchet, Lattice dynamics of α uranium, Phys. Rev. B 77 (2008) 024113. doi:10.1103/PhysRevB.77.024113.
URL `https://link.aps.org/doi/10.1103/PhysRevB.77.024113`

[109] J. C. Wojdeł, P. Hermet, M. P. Ljungberg, P. Ghosez, J. Í˜niguez, First-principles model potentials for lattice-dynamical studies: general methodology and example of application to ferroic perovskite oxides, Journal of Physics: Condensed Matter 25 (30) (2013) 305401.
URL `http://stacks.iop.org/0953-8984/25/i=30/a=305401`